Electronic Supplementary Information

Ionic-to-electronic current amplification in hybrid perovskite solar cells: ionically gated transistor-interface circuit model explains hysteresis and impedance of mixed conducting devices

Davide Moia[1†*], Ilario Gelmetti[2,3†*], Phil Calado[1], William Fisher[1], Michael Stringer[4], Onkar Game[4], Yinghong Hu[5], Pablo Docampo[5,6], David Lidzey[4], Emilio Palomares[2,7], Jenny Nelson[1], Piers R. F. Barnes[1*]

[1]Department of Physics, Imperial College London, London SW7 2AZ, UK
[2]Institute of Chemical Research of Catalonia (ICIQ), Barcelona Institute of Science and Technology (BIST), Avda. Països Catalans 16, 43007 Tarragona, Spain
[3]Departament d'Enginyeria Electrònica, Elèctrica i Automàtica, Universitat Rovira i Virgili, Avda. Països Catalans 26, 43007 Tarragona, Spain
[4]Department of Physics and Astronomy, University of Sheffield, Sheffield S3 7RH, UK
[5]Department of Chemistry and Center for NanoScience (CeNS), LMU München, Butenandtstrasse 5-13, 81377 München, Germany
[6]Physics Department, School of Electrical and Electronic Engineering, Newcastle University, Newcastle upon Tyne NE1 7RU, UK
[7]ICREA, Passeig Lluís Companys, 23, Barcelona, Spain

* davide.moia11@imperial.ac.uk
* igelmetti@iciq.es
* piers.barnes@imperial.ac.uk
† These authors contributed equally to this study

Table of Contents

Page

Supplementary Methods

Supplementary Notes

Methods 1 Device Fabrication

1.1 Spiro-OMeTAD/ $Cs_{0.05}FA_{0.81}MA_{0.14}PbI_{2.55}Br_{0.45}/TiO_2$ (Fig. 2)

Chemicals: Lead (II) Iodide (PbI_2, 99.99%), Lead Bromide ($PbBr_2$) were purchased from TCI UK Ltd. Formamidinium Iodide (FAI), Methylammonium Bromide (MABr), FK209 Co(III) TFSI and 30NTD TiO_2 paste were purchased from Greatcell Solar. Dimethylformamide (DMF anhydrous), Dimethyl sulfoxide (DMSO, anhydrous), Chlorobenzene (anhydrous), Acetonitrile (anhydrous), Titanium di-isopropoxide bis-acetylacetonate (TiPAcAc, 75 wt% in IPA), Butyl Alcohol (anhydrous), Bis(trifluoromethane)sulfonimide lithium salt (Li-TFSI), 4-tert-butyl pyridine (96%), Cesium Iodide (99.9%) were purchased from Sigma Aldrich. Spiro-MeOTAD (Sublimed grade 98%) and Fluorine doped Tin Oxide (FTO, 8Ω/□) substrates were purchased from Ossila Ltd. UK. All chemicals were used without further purification.

FTO substrates were patterned to desired geometry using chemical etching with Zinc metal powder and Hydrochloric Acid (4M, Sigma Aldrich). Substrates were cleaned by sequential ultra-sonication in diluted Hellmanex (Sigma Aldrich), Deionised water and Isopropyl-Alcohol. Compact-TiO_2 layer (~30 nm) was deposited on patterned FTOs using spray pyrolysis of TiPAcAc (0.5 M in butyl alcohol) at 450 °C and post-heated at 450 °C for 30 min. Mesoporous TiO_2 layer (~150 nm) was then deposited by spin coating 30NRD solution (1:6 wt:wt in butyl alcohol) at 5000 RPM for 30 s and heated at 150 °C for 10 min. Substrates were then heat-treated at 480 °C for 30 min to remove organic contents in the 30-NRD paste.

Triple cation ($Cs_{0.05}FA_{0.81}MA_{0.14}PbI_{2.55}Br_{0.45}$) perovskite solution was prepared using a reported protocol[1]. CsI, FAI, MABr, PbI_2 and $PbBr_2$ were mixed in appropriate ratio in mixed solvents DMF:DMSO (4:1 v:v) to get 1.2 M concentration of Pb^{2+} ions. This solution was filtered using 0.4 μm PTFE syringe filter before use. Perovskite films were deposited by anti-solvent quenching method in which 70 μL solution was spin coated initially at 2000 RPM for 10 s (ramped 200 RPM s^{-1}) and then at 6000 RPM for 20 s (ramp 2000 RPM s^{-1}) with 100 μL chlorobenzene dripped at 10 s before the end of second spin cycle. Spin coated perovskite films were crystalised by heating at 100 °C for 30 min. After cooling, hole-transport layer (HTL) of spiro-OMeTAD was spin coated at 4000 RPM for 30 s. HTL solution was prepared by dissolving 86 mg spiro-OMeTAD (Ossila Ltd. sublime grade) in 1 mL chlorobenzene, Li-TFSI (20 μL from 500 mg mL^{-1} stock solution in Acetonitrile), FK209 Co-TFSI (11 μL from 300 mg mL^{-1} stock solution in acetonitrile) and tert-butyl pyridine (34 μL). HTL coated perovskite cells were aged in dry air (RH < 20 %) for 12 hours before depositing Au (80 nm) top electrodes using thermal evaporation. Fabricated devices were then encapsulated first using 250 nm Al_2O_3 deposited by e-beam process and then using UV-Vis curable epoxy (Ossila Ltd.) with glass cover-slip. The thickness of the perovskite layer was 550 ±20 nm. The active area of the device was 0.12 cm^2.

1.2 Spiro-OMeTAD/ $FA_{0.85}MA_{0.15}PbI_3$ /SnO_x (Fig. 5a)

For the fabrication of perovskite solar cell on an SnO_x compact layer, patterned and cleaned FTO-glass (7Ω/sq, Hartfordglass Inc.) was covered with a 10 nm SnO_x layer using an atomic layer deposition (ALD) process. Tetrakis(dimethylamino)tin(IV) (TDMSn, Strem, 99.99%) was used as a tin precursor and held at 75 °C during depositions. The deposition was conducted at 118 °C with a base pressure of 5 mbar in a Picosun R-200 Advanced ALD reactor. Ozone gas was produced by an ozone generator (INUSA AC2025). Nitrogen (99.999%, Air Liquide) was used as the carrier and purge gas with a flow rate of 50 sccm per precursor line. The growth rate was 0.69 Å per cycle. Double cation ($FA_{0.85}MA_{0.15}PbI_3$) perovskite solution was prepared by dissolving FAI (182.7 mg, 1.06 mmol), MAI (29.8 mg, 0.19 mmol) and PbI_2 (576.2 mg, 1.25 mmol) in a mixture of 800 µL DMF and 200 µL DMSO. The solution was filtered using a 0.45 µm PTFE syringe filter before use. $FA_{0.85}MA_{0.15}PbI_3$ perovskite films were prepared on the compact SnO_x layer by spin-coating 75 µL solution at first 1000 rpm, then 5000 rpm for 10 s and 30 s, respectively. 500 µL chlorobenzene was dripped as an anti-solvent 15 s before the end of the second spin cycle. Spin-coated perovskite films were annealed at 100 °C for 10 min. For the hole transporter layer, 1 mL of a solution of spiro-OMeTAD (Borun Chemicals, 99.8%) in anhydrous chlorobenzene (75 mg mL^{-1}) was doped with 10 µL 4-*tert*-butylpyridine and 30 µL of a Li-TFSI solution in acetonitrile (170 mg mL^{-1}) and deposited by spin-coating at 1500 rpm for 40 s and then 2000 rpm for 5 s. After storing the samples overnight in air at 25% relative humidity, 40 nm Au was deposited through a patterned shadow mask by thermal evaporation. The devices were encapsulated using epoxy (Liqui Moly GmbH) and glass cover-slips. The active area was 0.158 cm^2 for the impedance measurements.

Methods 2 Device characterisation

2.1 Photovoltaic measurements

The current-voltage characteristics of the spiro-OMeTAD/$Cs_{0.05}FA_{0.81}MA_{0.14}PbI_{2.55}Br_{0.45}$/$TiO_2$ device was measured with forward and backward scans between -0.1 V to 1.2 V with scan rate of 400 mV s^{-1} under a Newport 92251A–1000 AM 1.5 solar simulator calibrated against an NREL certified silicon reference cell. An aperture mask of 0.0261 cm^2 was used to define the active area, see Fig. S8a. The performance of the spiro-OMeTAD/ $FA_{0.85}MA_{0.15}PbI_3$/SnO_x device is shown in Fig. S8b. An identical spiro-OMeTAD/$Cs_{0.05}FA_{0.81}MA_{0.14}PbI_{2.55}Br_{0.45}$/$TiO_2$ device showed good stability when aged using an ATLAS Suntest CPS+ solar simulator with a 1500 W xenon lamp and internal reflector assembly to provide continuous illumination (~100 mW cm^{-2}) to the unmasked device for 40 hours. Current-voltage measurements were made every 10 minutes (reverse sweep 1.15 V to 0V) in lifetime tester, see Fig. S8c.

2.2 Impedance measurements

Impedance measurements were performed using an Ivium CompactStat potentiostat. The perovskite solar cell devices were masked using an aperture slightly bigger than the total active area defined by the overlap between the FTO layer and the top metal contact. All impedance measurements were run by applying a 20 mV sinusoidal voltage perturbation to the cell superimposed on a DC voltage. The potentiostat measures the resulting current, this is used to calculate the impedance spectrum as described in the main text. The frequency of the perturbation was varied between 1 MHz to 0.1 Hz. The measurement was performed after a stabilisation time of at least 100 seconds at the (light and voltage) bias condition used in the measurement, unless stated otherwise. When different stabilisation protocols were used to investigate the effect of preconditioning on the impedance measurements, these are specified in the figure legends. Different bias light conditions were obtained using white LEDs and the sun equivalent light intensity was using a filtered silicon photodiode calibrated by an AM1.5 solar simulator. Stabilisation of the cell was performed as follows. Chronopotentiometry (for impedance measurements under light at open circuit) or chronoamperometry (for impedance measurements under light at short circuit or in the dark with an applied potential bias) measurements were collected before the stabilisation stage to monitor the cell behaviour while settling to the set measurement condition. For each measurement at open circuit under light, we ran a chronopotentiometry measurement and we used the open circuit voltage measured after at least 100 seconds as the DC voltage bias condition during the impedance measurement. This voltage was applied for an additional 100 seconds before the beginning of the impedance measurement. For measurements at short circuit under light or at an applied potential in the dark, a chronoamperometry measurement was run for 100 seconds to monitor the evolution of the current in the device at the applied voltage. The same voltage was then applied for additional 100 seconds before the start of the impedance measurement. In some cases we noticed that changes in cell potential or current still occurred after 100 second stabilisation time. One could expect that these slow variations would not significantly vary the features probed at frequencies that range down to about 10 times the inverse of the stabilisation time (in our case about 0.1 Hz). However, we found that this is not the case. In particular, some peculiar features (loops in the Nyquist plots) disappeared after sufficiently long stabilisation (see Fig. S2a-d). While these features might still be indicative of the state of the device at the time of the measurement, they represented a transient state rather than the equilibrated state. For measurements at quasi-equilibrium the influence of different stabilisation times should be recorded to assess the influence on a feature of interest in an impedance spectrum to identify the minimum time needed for the spectra to reach acceptable convergence.

Methods 3 Drift-diffusion simulation of impedance measurements

Driftfusion is a one-dimension drift-diffusion simulation for modelling perovskite solar cells which solves for the time-dependent profiles of free electron, free hole, mobile ion and electrostatic potential. The device physics of the model are based on established semi-classical transport and continuity equations, which are described in reference 1 of the main text. The code uses MATLAB's built-in Partial Differential Equation solver for Parabolic and Elliptic equations (PDEPE) to solve the continuity equations and Poisson's equation for electron density n, hole density p, a positively charged mobile ionic charge density a, and the electrostatic potential V as a function of position x and time t. Positively charged mobile ions and a negatively charged static counter ions (simulating Shottky defects[2]) are confined to the intrinsic region in order to simulate the high density of mobile defects in the perovskites. High rates of recombination in the contact regions are used to simulate surface/interfacial recombination.

In order to deal with the high charge density and electrostatic potential gradients at the interfaces a piece-wise linear spatial mesh was used with a spacing of 2.54 nm outside of, and 0.55 nm within the approximate depletion regions of the device. The time mesh was evaluated with either linearly or logarithmically spaced points dependent on predicted gradients in the time dimension. A complete description of the model is given in the supporting information of reference 25. Interfacial recombination (SRH) was defined to occur within a region ± 2nm from the perovskite interfaces. The code used for simulation can be downloaded from: https://github.com/barnesgroupICL/Driftfusion where usage examples specific to impedance spectroscopy are reported in the included documentation.

For simplicity we used electron and hole transporting contacts with the same band-gap, but work functions that differ from the intrinsic perovskite, to create a built-in potential in the simulated perovskite layer. Illumination was described by a uniform rate of charge generation throughout the active layer also for simplicity.

The solution of the charge and electrostatic concentration profiles of the device under steady state operating conditions was determined to provide initial conditions for the simulated impedance spectroscopy. The impedance spectroscopy simulations were performed by applying an oscillating voltage, v, with amplitude, v_{max} = 2 mV superimposed on a bias voltage $\bar{V}$ boundary condition:

$$\bar{V} + v = \bar{V} + v_{max} \cdot \sin(\omega t)$$

where ω = 2π×frequency. For measurement of the device around its open circuit potential, $\bar{V}$ was set to the equilibrated value of V_{OC} at steady state.

The electronic current was then estimated from the solution via the continuity equations. Usually a simulation of 20 voltage periods (evaluated with 40 time points per period) was enough for extracting the impedance information from the current profile.

The amplitude and phase of the oscillating electronic current density was obtained via demodulation, mimicking the working principle of a two-phase lock-in amplifier. The current density profile was point-by-point multiplied by the voltage profile or the π/2 rad shifted voltage profile normalised by v_{max} and integrated over time (typically 10 periods):

$$X = \frac{\omega}{m\pi} \int_{t_0}^{t_0 + \frac{2m\pi}{\omega}} j(t) \cdot \sin(\omega t) dt$$

$$Y = \frac{\omega}{m\pi} \int_{t_0}^{t_0 + \frac{2m\pi}{\omega}} j(t) \cdot \cos(\omega t) dt$$

where m is the number of periods, and t_0 is the start of the integration time. The amplitude and phase are then given via:

$$j_{max} = \sqrt{X^2 + Y^2}$$
$$\theta = \arctan\left(\frac{Y}{X}\right)$$

allowing the impedance to be determined by $Z = {}^{v_{max}}/_{j_{max}} \exp(-i\theta)$. The amplitude and phase obtained this way were confirmed by fitting $j(t)$ with a sinusoidal function.

To analyse of the output of the simulation, both the electronic accumulation current and the ionic displacement current were evaluated from the solutions for the time dependent concentration profiles of electrons, holes, and ions (see Fig. 2). The ionic displacement current, J_{ion}, in the device was evaluated by determining the electric field profile due only to ions E_{ion} as a function of time:

$$E_{ion}(x,t) = \frac{q}{\varepsilon_0 \varepsilon_r} \int_{x_1}^{x_1 + x} a(x',t) dx'$$

then finding its average value as a function of time:

$$\langle E_{ion}(t) \rangle = \frac{1}{d_{prv}} \int_{x_1}^{x_2} E_{ion}(x,t) dx$$

to calculate the corresponding displacement current:

$$J_{ion} = -\varepsilon_0 \varepsilon_r \frac{\partial \langle E_{ion}(t) \rangle}{\partial t}.$$

Where $a(x,t)$ is the ionic concentration profile, x is the position in the device, x_1 is the position of the HTL/perovskite interface, x_2 the position of the perovskite/ETM interface, q is the elementary charge, $\varepsilon_0 \varepsilon_r$ is the perovskite permittivity.

The total accumulation current, j_{acc}, (which includes the electronic charge in the contacts compensating ionic charge in the perovskite) was determined by subtracting the net recombination current (recombination minus generation) from the total cell current:

$$j_{acc}(t) = j(t) - j_{rec}(t) + j_{gen}(t)$$

where $j_{\mathrm{rec}}(t)$ and $j_{\mathrm{gen}}(t)$ were evaluated by integrating the recombination/generation terms in the current continuity equations over the device thickness using electron and hole concentration profiles. The parameters used in the simulation are listed in Table S2, unless stated otherwise.

Methods 4 Equivalent circuit model

We now describe the expressions underlying the equivalent circuit model, and the approach to fitting the data. We will initially focus on the fit to data in Fig. 2. If a single interfacial electron or hole transfer process is assumed to dominate the observed impedance of the device (see discussion in Note S6) then the quasi Fermi potentials of the electrons or holes, V_{n} or V_{p}, may be set to 0 or V and an equivalent circuit of the following form can be used to fit to the experimental data (this example is for electron recombination so we can set $V_{\mathrm{n}} = 0$ V). The appropriate equivalent circuit, arbitrarily only considering electrons, is given in Fig. 2e. The impedance of the circuit is given by:

$$Z = \left(\frac{1}{Z_{ion}} + \frac{1}{Z_{rec}}\right)^{-1}$$

where Z_{ion} is the impedance of the ionic circuit branch and Z_{rec} is the impedance of the electronic circuit branch, in this case specifically for the limiting process of recombination. The expressions for this simple case of these terms are presented in Table 1 of the main text, but their origins are described in more detail below.

4.1 Impedance of the ionic circuit branch

Z_{ion} is determined by drawing an analogy with the Debye relaxation of a lossy dielectric material (the perovskite) between two conducting plates (representing the undepleted regions of the device contacts) where the dependence of the effective complex permittivity of the medium between the plates varies with the angular frequency (ω) as:

$$\varepsilon(\omega) = \varepsilon_\infty + \frac{\varepsilon_S - \varepsilon_\infty}{1 - i\omega\tau_{ion}}.$$

In this expression ε_∞ represents the effective permittivity of the material between the conducting plates if no mobile ions were present or when ω is too high for the ions move. The capacitance per unit area of this device at high frequency (excluding any interfacial charge transfer effects discussed elsewhere in this study) would then be given by $C_g = \varepsilon_\infty / d_g$ where d_g is the combined thickness of the perovskite layer and the space charge layers in the contacts (see upper panel of Fig. 4f where $\omega \rightarrow \infty$). The term ε_s represents the effective permittivity of the medium sandwiched between the plates at sufficiently low angular frequencies that the perovskite layer is fully polarised by the accumulation of mobile ions to screen the applied potential (see lower panel of Fig. 4f where $\omega \rightarrow 0$). In this case the measured capacitance of the device (again excluding any interfacial charge transfer effects) will be related to ε_s by: $C_{ion}/2 = \varepsilon_s / d_g$ where C_{ion} is the capacitance of the space charge region surrounding each of the two contact/perovskite interfaces so $C_{ion} = \varepsilon_{sc}/d_{sc}$ where ε_{sc} is permittivity of the interfacial space charge region and d_{sc} is its thickness (for simplicity here we assume the capacitance of each interface is similar so the device capacitance is given by the capacitors in series $\left[C_{ion}^{-1} + C_{ion}^{-1}\right]^{-1}$). The time constant for ionic redistribution is given by $\tau_{ion} = R_{ion}C_{ion}/2$ where R_{ion} is the specific resistance to ion motion across the perovskite layer (related to the perovskite ionic conductivity by $\sigma_{ion} \approx d_g / R_{ion}$ (if $d_{sc} << d_g$) so that $\tau_{ion} \approx \varepsilon_s / \sigma_{ion}$ as recently highlighted by Jacobs *et al.* in reference 33 in the main text.

The complex capacitance of the device due to the ionic branch of the circuit as a function of frequency is then given by $\varepsilon(\omega)/d_g$ from which we can derive an expression for the impedance of the ionic branch of the circuit:

$$Z_{ion} = \left[i\omega C_g + \frac{i\omega\left(C_{ion}/2 - C_g\right)}{1 + i\omega R_{ion}C_{ion}/2}\right]^{-1}.$$

We have depicted this frequency dependent ionic branch of the device's circuit in Fig. 4f as a C_{ion}–R_{ion}–C_{ion} series curly bracketed by C_g in other figures both for compactness and to maintain the physical meaning of the circuit elements. The parameters R_{ion} and C_{ion} can easily be determined by fitting with an $(R_{eff}$–$\Delta C_{ion})||C_g$ equivalent circuit represented by the ionic circuit branch in Fig. 2f to the impedance data of a device at zero bias in the dark (assuming the impedance of the electronic circuit branch is large) and determining the parameters ΔC_{ion}, R_{eff} and C_g to give:

$$C_{ion} = 2(\Delta C_{ion} + C_g)$$

and

$$R_{ion} = \frac{R_{eff}\Delta C_{ion}}{\Delta C_{ion} + C_g}.$$

In cases where $C_{ion} \gg C_g$ then $\Delta C_{ion} \approx C_{ion}/2$ and $R_{eff} \approx R_{ion}$, however this will not hold when the space charge layers in either the perovskite or contacts are not much smaller than the perovskite thickness.

Note that we have not included a series resistance for the contacts in this model since its magnitude was negligible relative to the other elements under consideration under most measurement conditions, however we note that it is trivial to include (for example when fitting the data in Fig. 5a). As stated above, C_g is the geometric capacitance of the device at high frequency, and C_{ion} is the capacitance of the space charge regions of the interfaces (assumed here to be symmetric for both interfaces see Note S6, and Tables S3 and S4 for asymmetric cases) which results from the capacitance of the electronic and ionic space charge layers on either side of the interface in series. Both C_{ion} and C_g will show a dependence on the d.c. voltage $\bar{V}$ across the device which will change the width of the space charge layers according to the approximations:

$$C_{ion}(\bar{V}) \approx C_{ion}(\bar{V} = 0)\sqrt{\frac{V_{bi}}{V_{bi} - \bar{V}}}$$

and

$$C_g(\bar{V}) \approx \left[\frac{2}{C_{ion}(\bar{V} = 0)}\left(\sqrt{\frac{V_{bi} - \bar{V}}{V_{bi}}} - 1\right) + \frac{1}{C_g(\bar{V} = 0)}\right]^{-1}$$

where V_{bi} is the built-in potential of the device corresponding to the difference in work functions between the ETM and HTM contacts (or more generally between the perovskite and each contact material if calculating C_{ion} for each interface). If V_{bi} is known, or can be roughly estimated, it can be used as a constant input in the model, otherwise it can be used as an optional free fitting parameter. The value of V_{bi} has only a weak influence on the overall quality of the fit, and similar results will be achieved if C_{ion} and C_g are considered constant.

A more accurate description of the ionic branch of the circuit could be expanded to describe dispersive ionic transport, effects of a mesoporous layer, and diffusion of more than one mobile ionic species.

4.2 Impedance of the electronic circuit branch (dominated by recombination of one carrier type)

To determine the impedance of the electronic circuit branch it is necessary to find the effect of the electrostatic potential of the ions on the concentration of electronic charge in the perovskite. The expression for Z_{rec} can be derived following the arguments in the main text based on the interfacial transistor model, in this section, we confine to considering electron transfer across interface 1 which has an electrostatic potential of V_1 due to the ionic distribution. As discussed, the current across the interface, J_1, is approximated by the recombination current, J_{rec}:

$$J_1 \approx J_{rec} = J_{s1} \exp\left[qV_1/m_1 k_B T\right]$$

where J_{s1} is the saturation current density for the interface at equilibrium in the dark. To allow a more general description of the interfacial processes in real devices, we have included an ideality factor, m_1, describing the non-ideal variation of recombination current across interface 1 as a function of V_1. To find how J_{rec} varies with respect to the voltage V applied across the cell we must understand the relationship between V and V_1, the electrostatic potential due to the ions at the interface.

The ionic branch of the circuit discussed above contains the series of elements C_{ion}–R_{ion}–C_{ion}. When a voltage is applied across the circuit, the electrostatic potential at the HTM/perovskite interface relative to dark equilibrium, V_1, can be calculated from the potential drop across the remaining components in the series (R_{ion}–C_{ion}). To account for the interface being located within the space charge layer that spans the interface (the interface is located between the depletion layer in the contact and the ion accumulation layer in the perovskite, Fig. S1a) we introduce the term f_{c}. This parameterises the fraction of the electrostatic potential dropping across the interface which occurs within the contact layer to control the interfacial transfer process (in this case recombination). If recombination is localised only at the interface then $f_c \approx 1 - C_{ion}/C_{per} = C_{ion}/C_{con}$ where C_{per} is the capacitance due to the accumulation or depletion of ionic charge at the perovskite interface neglecting the space charge layer in the contact. The capacitance across the space charge layer in both the contact, C_{con}, and perovskite, C_{per}, contribute to the overall low frequency capacitance of the interface as $C_{ion} = \left[C_{con}{}^{-1} + C_{per}{}^{-1}\right]^{-1}$, see Figs S1a and S6. Consequently, f_{c} will be related to the relative permittivities and doping or ionic densities on either side of the interface as well as being weakly dependence on the spatial distribution of interfacial trap states. Here, for simplicity, we assume it is constant. For the C_{ion}–R_{ion}–C_{ion} series, the steady state d.c. voltage driving recombination across interface 1 will be given by:

$$\bar{V}_{rec} = V_1 - V_n = \frac{\bar{V}}{2}(2 - f_c)$$

assuming no drop in the electron quasi Fermi level at the opposite interface (V_{n} = 0). The electrostatic potential of the interface 1 in response to an applied d.c. voltage with a superimposed oscillation, $V = \bar{V} + v$, is given by considering the complex impedance of the C_{ion}–R_{ion}–C_{ion} series:

$$V_{rec} = V_1 = \frac{\bar{V}}{2}(2 - f_c) + \frac{v}{2}\left(2 - \frac{f_c}{1 - i\omega R_{ion}C_{ion}/2}\right).$$

Substituting this into the expression for J_{rec} above and differentiating with respect to V gives an expression for the electronic impedance of the recombination process, since when $V_{\mathrm{n}} = 0$, $\mathrm{d}J_{\mathrm{rec}}/\mathrm{d}V = 1/Z_{\mathrm{rec}}$:

$$Z_{rec} = \frac{2}{(2 - \frac{f_c}{1 + i\omega R_{ion}C_{ion}/2})}\frac{m_1 k_B T}{qJ_{rec}(\bar{V})}$$

The corresponding expressions for the other interface and cases where $V_n \neq 0$ (i.e. when the electron quasi Fermi level in the perovskite is not equal to the electron quasi Fermi level in the ETM) are given in Table S3. More general cases where the ionic capacitance is not equal at interface 1 and 2 are given in Table S4. Table 1 of the main text shows the expressions for the potential at each interface, V_1 and V_2, and the electronic impedance for this circuit branch for the simple case where $f_c = 1$.

The ideality factor for the recombination current at interface 1 as a function of V_{rec}, m_1, can be estimated from the steady state ideality factor, m_{ss}, determined from the slope of V_{OC} *vs* log(light intensity) measurements[35] using the following expression:

$$m_1 \approx m_{ss}\left(1 - \frac{f_c}{2}\right)$$

We can then evaluate the recombination current density across the interface at steady state with the expression:

$$J_{rec}(\bar{V}) = J_{s1}\exp\left(\frac{q\bar{V}_{rec}}{m_1 k_B T}\right) = J_{s1}\exp\left(\frac{q\bar{V}}{m_{ss} k_B T}\right)$$

Combining these concepts, the impedance of the recombination process in terms of the bias across the device, $\bar{V}$, and its steady state ideality factor, m_{ss}, becomes:

$$Z_{rec} = \frac{2}{(2 - \frac{f_c}{1 + i\omega R_{ion}C_{ion}/2})}\frac{m_{ss}\left(1 - \frac{f_c}{2}\right)k_B T}{qJ_{s1}\exp\left(\frac{q\bar{V}}{m_{ss} k_B T}\right)}$$

4.3 Impedance of the whole device

The complete expression for the impedance of the device can be calculated by considering the impedance of the ionic (Z_{ion}) and electronic (Z_{rec}) branches of the circuit model in parallel and including series resistance, R_{s}:

$$Z = R_s + \left\{ i\omega C_g(\bar{V}) + \frac{i\omega\left[C_{ion}(\bar{V})/2 - C_g(\bar{V})\right]}{1 + i\omega R_{ion}C_{ion}(\bar{V})/2} + \frac{1}{2}\left[2 - \frac{f_c}{1 + i\omega R_{ion}C_{ion}(\bar{V})/2}\right]\frac{qJ_{s1}\exp\left(\frac{q\bar{V}}{m_{ss}k_BT}\right)}{m_{ss}\left(1 - \frac{f_c}{2}\right)k_BT} \right\}^{-1}$$

The cell bias voltage, $\bar{V}$ and the steady state ideality factor, m_{ss}, are known or determined independently from measurements. $C_{ion}(\bar{V})$ and $C_g(\bar{V})$ will approximately depend on $\bar{V}$ as described above using an estimation of V_{bi}. The unknown device parameters in this expression for Z can be determined from a fit are: R_{s}, R_{ion}, $C_{ion}(\bar{V} = 0)$, $C_g(\bar{V} = 0)$, J_{s1} and f_{c}. If V_{bi} cannot be estimated, it can also be used as a fitting parameter. Since R_{s} is typically trivial to determine from the impedance spectra this leaves only five significant parameters to describe key device physics.

A similar approach can be used to express the impedance of the device for the more general circuit for example if both recombination and injection of electrons limit impedance as described the section above:

$$Z = R_s + \left(\frac{1}{Z_{ion}} + \frac{1}{Z_n}\right)^{-1}$$

where Z_{n} is the impedance of electronic current transfer through the device (given in Table S3). More generally for transfer of both electrons and holes with impedance Z_{np} (given in Table S4) the device impedance becomes:

$$Z = R_s + \left(\frac{1}{Z_{ion}} + \frac{1}{Z_{np}}\right)^{-1}$$

We emphasise again that under most circumstances only one electronic process is likely to dominate the electronic branches of the device impedance so such a generalisation will not normally be required to describe a device around particylar operating conditions. We also emphasise that the impedance of the ionic branch of the circuit, Z_{ion}, might differ from the expression presented above in some devices, for example if ions penetrate or react at interfaces, or if ion transport is dispersive, or if more than one mobile ionic species is present (Fig. 5a and

Methods 6). Additionally, diffusive transport of ions might occur within mesoporous regions of a device which could potentially be described by a Warburg element in series with R_{ion}.

Methods 5. Fitting the impedance spectra to an equivalent circuit model

Global fits of the impedance circuit model for Z (the electron recombination only model) to the experimental and simulated impedance spectra at all measured conditions presented in Fig. 2 and Fig. 5 were performed using a non-linear least squares fitting routine. We aimed to use the fewest parameters possible to give a reasonable representation of the data. For Fig. 2 the free parameters were R_{ion}, $C_{ion}(\bar{V}=0)$, $C_g(\bar{V}=0)$, J_{s1} and f_c. The bias voltage, $\bar{V}$, and measured ideality factor for each measurement were used as inputs. Relatively little co-variance was observed between the parameters for the overall shape of the resulting device impedance spectra, so the fits were performed in a stepwise fashion in which the range of frequencies over which each parameter was fit was limited to the regions of the spectra which responded to that particular parameter. $C_g(\bar{V}=0)$ was determined from the fit to the high frequency region of the dark, 0 V bias, spectrum. $C_{ion}(\bar{V}=0)$ was initially determined from the fit to the low frequency region of the dark, 0 V bias, spectrum. R_{ion}, J_{s1}, and f_c (the fraction of screening potential dropping within the contacts) were determined from the fit to all the spectra from low frequency to medium frequency. The fit parameters the Fig. 2 data are given in Table S1.

To estimate R_{ion} directly from the measured impedance data we can use the relationship outlined in equation 3:

$$\frac{j''_{rec}}{J_{ion}} = \frac{R_{ion}}{2} f_c g_{rec} = \frac{R_{ion}}{2} f_c \frac{qJ_{rec}(\bar{V})}{m_1 k_B T}$$

where j''_{rec}/j_{ion} at low frequency ($\omega \rightarrow 0$) is given by:

$$\frac{j''_{rec}}{J_{ion}} = \frac{2c_{rec}}{C_{ion}} = \frac{c(\bar{V},\omega \rightarrow 0) - c(\bar{V}=0,\omega \rightarrow 0)\sqrt{\frac{V_{bi}}{V_{bi}-\bar{V}}}}{c(\bar{V}=0,\omega \rightarrow 0)\sqrt{\frac{V_{bi}}{V_{bi}-\bar{V}}}}$$

and the recombination transconductance can be evaluated from:

$$g_{rec} = \frac{q\bar{J}_{rec}(\bar{V})}{m_1 k_B T} = \frac{q\bar{J}_{rec}(\bar{V})}{m_{ss}\left(1 - \frac{f_c}{2}\right) k_B T}$$

The *c* terms are given by the measured apparent capacitance, $c = \omega^{-1}Im(Z^{-1})$ at the high and low frequency limits and bias voltages indicated. If the measurement is made in the dark and recombination is assumed to dominate the electronic impedance then the cell current $\bar{J} \approx \bar{J}_{rec}$. If the measurement is made at open circuit then $\bar{J}_{rec} \approx J_{ph}$ which may be estimated from the short circuit current or the absorbed photon flux.

Methods 6. Circuit model resulting in inductive behaviour due to recombination at an interface where ions may penetrate, or undergo a reversible chemical reaction

If ionic defects penetrate or chemically react reversibly with an interface, this will result in an additional perturbation of the ionic distribution which may have a different time constant to $R_{\text{ion}}C_{\text{ion}}/2$ which could lead to inductive behaviour. For example, iodide ions might reversibly react with oxygen vacancies in an SnO_x contact. An equivalent circuit giving an approximate description of ion penetration or a reversible reaction is shown in Fig. 5a and Fig. S7:

R_{int} is the effective interfacial resistance to ion penetration or reaction, and C_{ch} is the effective chemical capacitance of the contact for the ions. Depending on the frequency range and values of the circuit elements, changes in V_2 may lead or lag changes in the applied potential V resulting in apparently capacitive or inductive behaviour. Note that for simplicity we approximated the geometric capacitance by including a separate C_{g} branch in this model. To determine the behaviour of the current flowing through this circuit the frequency dependence of V_2 must be determined by examining the ionic branch of the circuit which has an impedance:

$$Z_{ion} = \frac{1}{i\omega C_{ion}} + R_{ion} + \left(i\omega C_{ion} + \frac{1}{R_{int} + \frac{1}{i\omega C_{ch}}} \right)^{-1}$$

Ignoring R_{S}, at steady state the potentials at V_1 and V_2 where $\omega \to 0$ will be given by:

$$\bar{V}_1 = \bar{V}_2 = \frac{C_{ion}}{2C_{ion} + C_{con}}\bar{V}$$

This allows the transconductance for hole recombination to be calculated given the voltage driving recombination is $\bar{V} - \bar{V}_2$ (see Table S4):

$$g^p_{rec} = \frac{q}{k_BT}J_{s2}e^{\frac{q(\bar{V} - \bar{V}_2)}{k_BT}} = \frac{q}{k_BT}J_{s2}e^{\frac{q}{k_BT}\left(1 - \frac{C_{ion}}{2C_{ion} + C_{ch}}\right)\bar{V}} = \frac{q\bar{J}^p_{rec}}{k_BT}$$

The small perturbation potentials v_1 and v_2 in response to v are then given by:

$$v_1 = \left(1 - \frac{1}{i\omega C_{ion} Z_{ion}}\right) v$$

$$v_2 = \left(1 - \frac{1}{i\omega C_{ion} Z_{ion}} - \frac{R_{ion}}{Z_{ion}}\right) v \,.$$

When a small perturbation *v* is applied across the interface the voltage driving recombination *v* - v_2 can be found using the above expression. This enables the impedance to hole current recombining across the interface to be found by dividing $j_{rec}^{p} = (v - v_2) g_{rec}^{p}$ by *v*:

$$\frac{1}{Z_{rec}^{p}} = \frac{j}{v} = \left(\frac{1}{i\omega C_{ion} Z_{ion}} + \frac{R_{ion}}{Z_{ion}}\right) \frac{qJ_{rec}^{p}}{k_B T}$$

This can then be incorporated within the complete equivalent circuit to give the impedance of the device with the approximation that C_g is connected in parallel to Z_{ion} and including series resistance R_s:

$$Z = R_s + \left(i\omega C_g + \frac{1}{Z_{ion}} + \frac{1}{Z_{rec}^{p}}\right)^{-1}$$

$$Z = R_s + \left(i\omega C_g + \left[\frac{1}{i\omega C_{ion}} + R_{ion} + \left(i\omega C_{ion} + \frac{1}{R_{ion} + \frac{1}{i\omega C_{ch}}}\right)^{-1}\right]^{-1} + \left(\frac{1}{i\omega C_{ion} Z_{ion}} + \frac{R_{ion}}{Z_{ion}}\right) \frac{qJ_{rec}^{p}}{k_B T}\right)^{-1}$$

This expression can then be used in a global fit to the data.

Supplementary Notes

Note S1. Evaluation of inductive behaviour due to injection and negative ionic-to-electronic current transcarrier amplification

We now demonstrate that the circuit model can result in inductive behaviour due to interfacial charge injection processes coupled to ionic redistribution. Charge injection of a carrier (free electron or hole) will occur in series with the corresponding recombination process described above. Considering the electronic current across the ETM interface 2, the net current density is given by the difference between the injection and collection currents, J_{inj} and J_{col}:

$$J_2 = J_{inj} - J_{col} = J_{s2} e^{\frac{qV_{inj}}{k_B T}} - J_{s2} e^{\frac{qV_{col}}{k_B T}}$$

where J_{s2} is the electron saturation current density of the interface at equilibrium in the dark and the changes in barrier potentials V_{inj} and V_{col} in relation to ionic redistribution are given in Table 1, Fig. 4 and Fig. S4c.

If $V_{\mathrm{n}} \approx V$ (which, given our assumptions, would hypothetically occur under forward bias in the dark where $J_{\mathrm{s2}} >> J_{\mathrm{s1}}$) then the electron collection current is negligible and the impedance of interface 2 is controlled by injection (Table 1):

$$\frac{1}{Z_{inj}} = \frac{dj_{inj}}{dv} = \frac{1}{2}\left(\frac{1}{1 + i\omega R_{ion} C_{ion}/2}\right)\frac{qJ_{inj}(\bar{V})}{k_B T}$$

Comparing this with equation 3 shows that ionic motion causes Z_{inj} to vary with an imaginary component π rad out of phase with Z_{rec} so that the interface will behave like an inductor despite no release of accumulated electronic charge. The real part of this Z_{inj} is given by:

$$r_{inj} = Z'_{inj} = \frac{2k_B T}{qJ_{inj}(\bar{V})}$$

The corresponding negative value of the imaginary part of Z_{inj} divided by the angular frequency gives an expression which is analogous to an apparent inductance to injection l_{inj} of charge carriers across the interface:

$$l_{inj} = -\frac{Z''_{inj}}{\omega} = \frac{k_B T R_{ion} C_{ion}}{qJ_{inj}(\bar{V})}$$

This has the potential to lead to loops in Nyquist plots (Fig. S4c). As discussed in the main text, this result also implies the presence of a transcarrier amplification factor based on the following argument. At low frequency when $\omega \ll (R_{ion}C_{ion}/2)^{-1}$ the ionic current will be out of phase with v is given by $J_{ion} \approx i\omega C_{ion}v/2$ so that the out of phase component of the voltage perturbation at interface 2 is $v_2'' = -J_{ion}R_{ion}/2$ due to the electrostatic drop in potential across the perovskite. This results in an out of phase electronic current of $j_{inj}'' = -J_{ion}R_{ion}g_{inj}$ where g_{inj} is the injection transconductance of the interface given by $dJ_{inj}/dV_2 = qJ_{\mathrm{inj}}(\bar{V})/(k_{\mathrm{B}}T)$. Taking the ratio of these currents gives the ionic-to-electronic transcarrier amplification of the ionic current as mentioned in the main text:

$$\frac{j_{inj}''}{J_{ion}} = -R_{ion}g_{inj} = -R_{ion}\frac{qJ_{inj}(V,\omega = 0)}{k_BT}$$

Note S2. Calculating the impedance of both interfaces considering only electrons

In cases where the impedance of both interface 1 and interface 2 are comparable, the value of V_{n} will no longer be $V_{\mathrm{n}} \approx 0$ (for a recombination dominated impedance) or $V_{\mathrm{n}} \approx V$ (for injection dominated impedance) so it must be determined in order to quantify Z_1 and Z_2. The inclusion of both $Z_{\mathrm{rec}}(V,J_{\mathrm{ph}},\omega)$ (capacitor-like) and $Z_{\mathrm{inj}}(V,J_{\mathrm{ph}},\omega)$ (inductor like) elements within an equivalent circuit model can result in loops within Nyquist plots under some circumstances (see Fig. S4d). Table S3 (which is a more complete extension of Table 1) summarises the changes in potential barriers, electrostatic interface potentials, and small perturbation impedances considering electrons only. The value of V_{n} is evaluated by substituting the expressions for the interfacial currents at steady state (i.e. $\omega = 0$) in Table S3 into the following current continuity equation for the electronic interfacial currents using the steady state values of $\bar{V}_1$ and $\bar{V}_2$ where $\bar{V}_1 = \bar{V}_2 = \bar{V}/2$ (if $f_{\mathrm{c}} = 1$):

$$J_n = J_{rec} - J_{gen} + J_{ph} = J_{inj} - J_{col}$$

and solving numerically for V_{n}. In the small perturbation regime current continuity must also be obeyed so that:

$$j_n = j_{rec} - j_{gen} = j_{inj} - j_{col}$$

where the photogeneration current need not be considered as it is not perturbed. The above expression can be rewritten in terms of the product of the voltage perturbation driving each process (Table S3) with the transconductance for each process as:

$$j_n = v(1 - A - B_n)\frac{J_{rec}}{k_BT} + vA\frac{J_{gen}}{k_BT} = vA\frac{J_{inj}}{k_BT} - v(B_n - A)\frac{J_{col}}{k_BT}$$

where $B_n = v_n/v$. Since A is known (as defined in Table S3), this can be solved for B_{n} to give:

$$B_n = \frac{J_{rec} + A(J_{gen} - J_{rec} + J_{col} - J_{inj})}{J_{rec} + J_{col}}$$

The small perturbation impedance (for electrons) of the two interfaces in series can then be found by dividing *v* by j_{n} to give:

$$Z_n = Z_1 + Z_2 = \left((1 - A - B_n)\frac{J_{rec}}{k_B T} + A\frac{J_{gen}}{k_B T}\right)^{-1}$$

The impedances of each interface and individual process are separately listed in Table S3 (which also includes the process ideality factors) should they need to be evaluated separately. Almost identical arguments can be used if only hole processes dominate the impedance of the device. Bulk recombination can also be easily included by adding the appropriate expression to the current continuity equation as described for the general case in the Note S6, Table S4, and Fig. S8.

Note S3. Accounting for accumulating electronic charge in the perovskite layer

The model we have proposed assumes that the concentration of electronic charge in the active layer is negligible relative to the background concentration of mobile ionic defects. Particularly at higher bias voltages the concentration of electronic charge may become comparable to the ionic charge. Since the electronic charge is highly mobile relative to the ionic defects it will rapidly move to screen changes in the ionic charge distribution. This will have the consequence of screening any modulation in the values of V_1 and V_2 and thus modulation out of phase components of interfacial charge transfer. To approximately describe this screening behaviour for a simplified model considering just electrons and ions we can modify the equivalent circuit as shown in Fig. S8d.

As the value of the screening capacitance, C_{n}, the amplitude of the modulation electrostatic potential by the ions at V_1 and V_2 is reduced, removing the amplification behaviour from the out of phase currents across the interfaces resulting so that the Nyquist plot returns to a single semicircle (see Fig. S8e). Additionally, this electronic screening capacitance, C_{n}, also contributes the increase in overall device capacitance at high frequencies as the bias voltage increases.

Note S4. Calculating large perturbation current-voltage sweep behaviour

The time varying potential in the perovskite layer close to each interface can be evaluated for large perturbations. For example, the current response of the device in response to a linear voltage sweep can be found by considering the ionic branch of the circuit and its coupling to the electron branch for the circuit shown in Fig. 4g.

A linear voltage sweep with scan rate s is applied across the device terminals results in charge Q_{ion} that accumulates at the interfacial capacitances C_{ion} with time, this can be found by solving the differential equation:

$$\frac{dQ_{ion}}{dt} = \frac{1}{R_{ion}}\left(V_{initial} + st - \frac{2Q_{ion}}{C_{ion}}\right)$$

with the initial condition that $Q_{ion}(t=0) = Q_0$ and $V(t=0) \ = \ V_{initial}$ as the initial potential:

$$Q_{ion}(t) = \frac{C_{ion}}{2}V_{initial} - sR_{ion}\left(\frac{C_{ion}}{2}\right)^2 + s\frac{C_{ion}}{2}t + \left(sR_{ion}\left(\frac{C_{ion}}{2}\right)^2 + Q_0 - V_{initial}\frac{C_{ion}}{2}\right)e^{-\frac{2t}{R_{ion}C_{ion}}}.$$

Q_0 is the initial charge on C_{ion} relative to equilibrium in the dark (at equilibrium in the dark we define $Q_0 = 0$). When the scan starts Q_0 need not be in equilibrium with V_{initial}, this is particularly relevant to cases where the cell is preconditioned with a forward bias prior to measurement. The electrostatic potentials at V_1 and V_2 are given by:

$$V_1(t) = V(t) - f_c\frac{Q_{ion}(t)}{C_{ion}}$$
$$V_2(t) = f_c\frac{Q_{ion}(t)}{C_{ion}}$$

assuming that the fraction of potential dropped in the contacts ($f_c = C_{ion}/C_{con}$) is the same on both sides. This allows the current through the interfaces to be calculated by numerically solving the following expression to give V_{n} and thus J_{n} by substituting in the expressions for interfacial currents and potentials given in Table S3 (assuming V_n it is not set to 0 for cases where injection is not limiting):

$$J_n(t) = J_{rec}(t) - J_{gen}(t) + J_{ph} = J_{inj}(t) - J_{col}(t)$$

If only one process limits the interfacial currents then the interfacial electron current, J_{n}, can be found more simply, for example if electron recombination limits the current through the interfaces (V_{n} = 0 V) and:

$$J_n(t) = \frac{J_{s1}}{k_BT}e^{f_c\frac{Q_{ion}(t)}{C_{ion}}\frac{q}{k_BT}}$$

The device current, J, can then be found from the sum of the ionic current, J_{ion}, the geometric charging current, J_g, and the interfacial electronic current J_{n}:

$$J(t) = J_n(t) + J_{ion}(t) + J_g(t)$$

For a linear voltage sweep with rate s these currents are:

$$J_{ion}(t) = s\frac{C_{ion}}{2} - \frac{2\left(sR_{ion}\left(\frac{C_{ion}}{2}\right)^2 + Q_0 - \frac{C_{ion}}{2}V_{initial}\right)}{R_{ion}C_{ion}}e^{-\frac{2t}{R_{ion}C_{ion}}}$$

$$J_g(t) = C_g\left(s - \frac{V_{initial}}{R_{ion}C_{ion}/2} + \frac{Q_0}{R_{ion}\left(C_{ion}/2\right)^2}\right)e^{-\frac{2t}{R_{ion}C_{ion}}}$$

Examples of the modelled J using this approach are shown in Fig. 5d and Fig. S6 for cyclic voltammograms, they show the resulting hysteresis in the current-voltage behaviour. These simulated current voltage sweeps based on the parameters determined from fitting the experimental impedance spectrum show very good agreement with the experimentally measured current voltage sweeps in Fig. S8a for the same scan rate.

Note S5. Calculating large perturbation current-voltage step behaviour

The response of the circuit to a voltage step may also be calculated by considering the response of the ions to a step change in cell potential from V_{initial} to V_{final}. The differential equation for the evolution of ionic charge is given by:

$$V_{final} - V_{initial} = R_{ion}\frac{dQ}{dt} + \frac{\left(2Q - C_{ion}V_{initial}\right)}{C_{ion}}$$

With the initial condition $Q(t = 0) = C_{ion}V_{initial}/2$, which has the solution:

$$Q_{ion}(t) = \frac{C_{ion}}{2}\left[V_{final} - \left(V_{final} - V_{initial}\right)e^{\frac{-2t}{R_{ion}C_{ion}}}\right]$$

The electrostatic potentials at V_1 and V_2 are given by:

$$V_1(t) = V_{final} - \frac{Q_{ion}(t)}{C_{ion}}$$

$$V_2(t) = \frac{Q_{ion}(t)}{C_{ion}}$$

Again, this allows the current through the interfaces to be calculated by numerically solving the following expression to give V_n and thus J_n (as described above for linear sweep voltammetry) by substituting in the expressions for interfacial currents and potentials given in Table S3:

$$J_n(t) = J_{rec}(t) - J_{gen}(t) + J_{ph} = J_{inj}(t) - J_{col}(t)$$

The currents in the other branches of the device circuit, J_{ion} and J_g are given by:

$$J_{ion}(t) = \frac{2(V_{final} - V_{initial})}{R_{ion}} e^{\frac{-2t}{R_{ion}C_{ion}}}$$

$$J_g \approx \frac{2(V_{final} - V_{initial})}{R_s} e^{\frac{-2t}{R_s C_g}}$$

Assuming that $R_s << R_{ion}$, giving $J(t) = J_n(t) + J_{ion}(t) + J_g(t)$. The resulting current (or photocurrent transients) may display apparently capacitive or inductive behaviour.

Note S6. General description of interfaces considering electrons, holes, bulk recombination, interface idealities, asymmetric ionic capacitance, partial ionic screening within the perovskite layer.

In the main text we assumed that under most circumstances a single electron or hole interfacial transfer process would dominate the observed impedance behaviour under a given operating condition. If the contributions to the impedance from the processes at all interfaces are considered then the total impedance of the combined interfaces will be given by:

$$Z_{np} = \left(\frac{1}{Z_1^n + Z_2^n} + \frac{1}{Z_1^p + Z_2^p}\right)^{-1}$$

where Z_1^n and Z_2^n are the electron transfer impedances of interfaces 1 and 2, and Z_1^p and Z_2^p are the corresponding hole transfer impedances (see Table S4). Note that in these expressions and those that follow the superscripts 'n' and 'p' are used to distinguish processes related electrons or holes, *they do not refer to exponents*. The value of Z_{np} will be dominated by the process with the highest impedance within the branch showing the lowest impedance, interface dominating impedance may vary for different operating conditions.

Under some circumstances more than one process may contribute to the observed impedance in which case a complete expression for Z_{np} may be evaluated. In the main text, and in the expression for Z_{np} above we also assumed that recombination only occurred at interfaces. We now describe the method to evaluate a more general version of the interface model, containing electrons, holes and bulk recombination (represented by a diode which describes recombination processes that depend only on the quasi Fermi level splitting such as band-to-band bimolecular recombination), see circuit diagram in Fig. S8f.

To find the impedance, the background steady state currents of each interfacial process must be established, this requires the values of V_n, V_p and J_np to be determined where J_np is the steady state electronic current due to both electrons and holes. We define the photogeneration current, J_ph to be negative. These quantities can be found by numerically solving a system of three simultaneous equations arising from Kirchhoff's laws:

$$J_{np} = J_{rec}^{n} - J_{gen}^{n} + J_{inj}^{p} - J_{col}^{p}$$
$$J_{np} = J_{rec}^{p} - J_{gen}^{p} + J_{inj}^{n} - J_{col}^{n}$$
$$J_{rec}^{n} - J_{gen}^{n} + J_{bulk} + J_{ph} = J_{inj}^{n} - J_{col}^{n}$$

with the appropriate expressions substituted into the terms which are given in Table S4. V_n, V_p and J_np allow the steady state interfacial currents to be evaluated and used to calculate the evaluate transconductances described below. Similar equations govern the current continuity in the small perturbation regime, without the need to include photocurrent (we note that the model could also be applied to describe intensity modulate photocurrent and photovoltage measurements (IMPS and IMVS) by including a small perturbation photocurrent):

$$j_{np} = j_{rec}^{n} - j_{gen}^{n} + j_{inj}^{p} - j_{col}^{p}$$
$$j_{np} = j_{rec}^{p} - j_{gen}^{p} + j_{inj}^{n} - j_{col}^{n}$$
$$j_{rec}^{n} - j_{gen}^{n} + j_{bulk} = j_{inj}^{n} - j_{col}^{n}$$

These can be rewritten in terms of the voltage perturbation driving each process and the corresponding transconductances:

$$\frac{1}{Z_{np}} = \frac{j_{np}}{v} = (1 - A_1 - B_n)\frac{qJ_{rec}^{n}}{m_1 k_B T} + A_1\frac{qJ_{gen}^{n}}{m_1 k_B T} + A_1\frac{qJ_{inj}^{p}}{m_1 k_B T} - (B_p + A_1 - 1)\frac{qJ_{col}^{p}}{m_1 k_B T}$$
$$\frac{1}{Z_{np}} = \frac{j_{np}}{v} = (B_p - A_2)\frac{qJ_{rec}^{p}}{m_2 k_B T} + A_2\frac{qJ_{gen}^{p}}{m_2 k_B T} + A_2\frac{qJ_{inj}^{n}}{m_2 k_B T} - (A_2 - B_n)\frac{qJ_{col}^{n}}{m_2 k_B T}$$
$$(1 - A_1 - B_n)\frac{qJ_{rec}^{n}}{m_1 k_B T} + A_1\frac{qJ_{gen}^{n}}{m_1 k_B T} + (B_p - B_n)\frac{qJ_{bulk}}{k_B T} = A_2\frac{qJ_{inj}^{n}}{m_2 k_B T} - (A_2 - B_n)\frac{qJ_{col}^{n}}{m_2 k_B T}$$

given that A_1 and A_2 are known (see Table S4) this system of equations can be solved analytically to give Z, B_n and B_p where $B_\mathrm{n} = v_\mathrm{n}/v$ and $B_\mathrm{p} = v_\mathrm{p}/v$. Here, Z_np is the impedance of the two interfaces in series for electrons and holes. The resulting analytical solutions are rather long and thus not reproduced here, however they are straightforward to evaluate using analytical mathematics software. The impedances of the individual processes and interfaces are listed in Table S4.

Supplementary references

1. H. Tan, A. Jain, O. Voznyy, X. Lan, F. P. García de Arquer, J. Z. Fan, R. Quintero-Bermudez, M. Yuan, B. Zhang, Y. Zhao, F. Fan, P. Li, L. N. Quan, Y. Zhao, Z.-H. Lu, Z. Yang, S. Hoogland and E. H. Sargent, *Science*, 2017, **355**, 722-726.
2. A. Walsh, D. O. Scanlon, S. Chen, X. G. Gong and S.-H. Wei, *Angewandte Chemie (International Ed. in English)*, 2015, **54**, 1791-1794.
3. J. J. Ebers and J. L. Moll, *Proceedings of the IRE*, 1954, **42**, 1761-1772.

Supplementary Figures

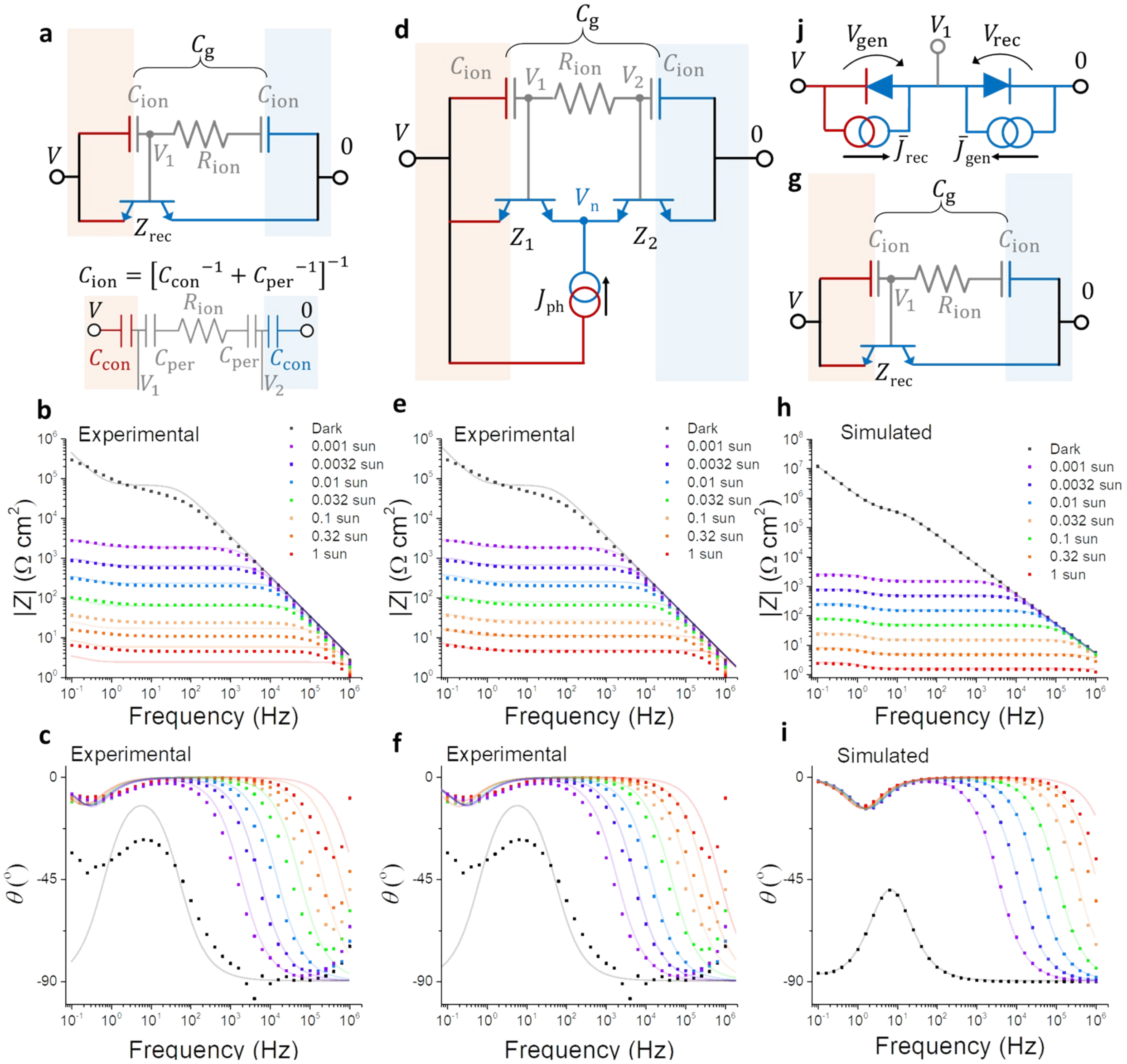

Fig. S1 Complete measured and simulated impedance spectra corresponding to Fig 2 with equivalent circuit model fits. The solid lines show the global fit to the measured and simulated data sets using the parameters listed in Table S1. **a-c**, The circuit model and measured impedance for the spiro-OMeTAD/ $Cs_{0.05}FA_{0.81}MA_{0.14}PbI_{2.55}Br_{0.45}/TiO_2$ solar cell in Fig. 2a and b and 5 free parameter global fit. At low frequencies it is apparent that the contribution from the transport of ionic defects is somewhat dispersive (ion movement with a range of time constants) whereas the circuit model and simulations assume non-dispersive transport. Some of the dispersive behaviour may be related to the presence of a thin (150 nm) mesoporous TiO_2 layer in this device which is not accounted for in the simulation or circuit model. Fine tuning the details of the ionic conduction model in the device and simulation would enable more precise characterisation of measured devices. The deviation of the fits at higher light intensities is likely to be related to either electronic screening of the interfaces by photogenerated charge (Note S3, ESI) and/or an increasing contribution from injection/collection impedance to the measured impedance. The lower panel of **a** shows the detailed capacitive contributions to C_{ion} from the space charge layer of the contact, C_{con}, and the ionic accumulation layer in the perovskite, C_{per}, as well as the consequences for determining the electrostatic potential at the interfaces, V_1 and V_2, if C_{con} and C_{per} are of comparable magnitudes instead of when $C_{ion} \approx C_{con}$ as is implicitly assumed in the upper part of the panel. **d-f,** Circuit model and 6 free parameter global fit to the experimental data in **b** and **c** including photogeneration (where J_{ph} is defined to be negative) and an injection/collection transistor element. **g-i**, Circuit model and 5 free parameter global fit to the simulated measurements in Fig. 2c and d. The global fit parameters for each case are given in Table S1. **j**, Ebbers-Moll representation[3] of the transistor model of interface 1 assuming infinite ionic-to-electronic current gain.

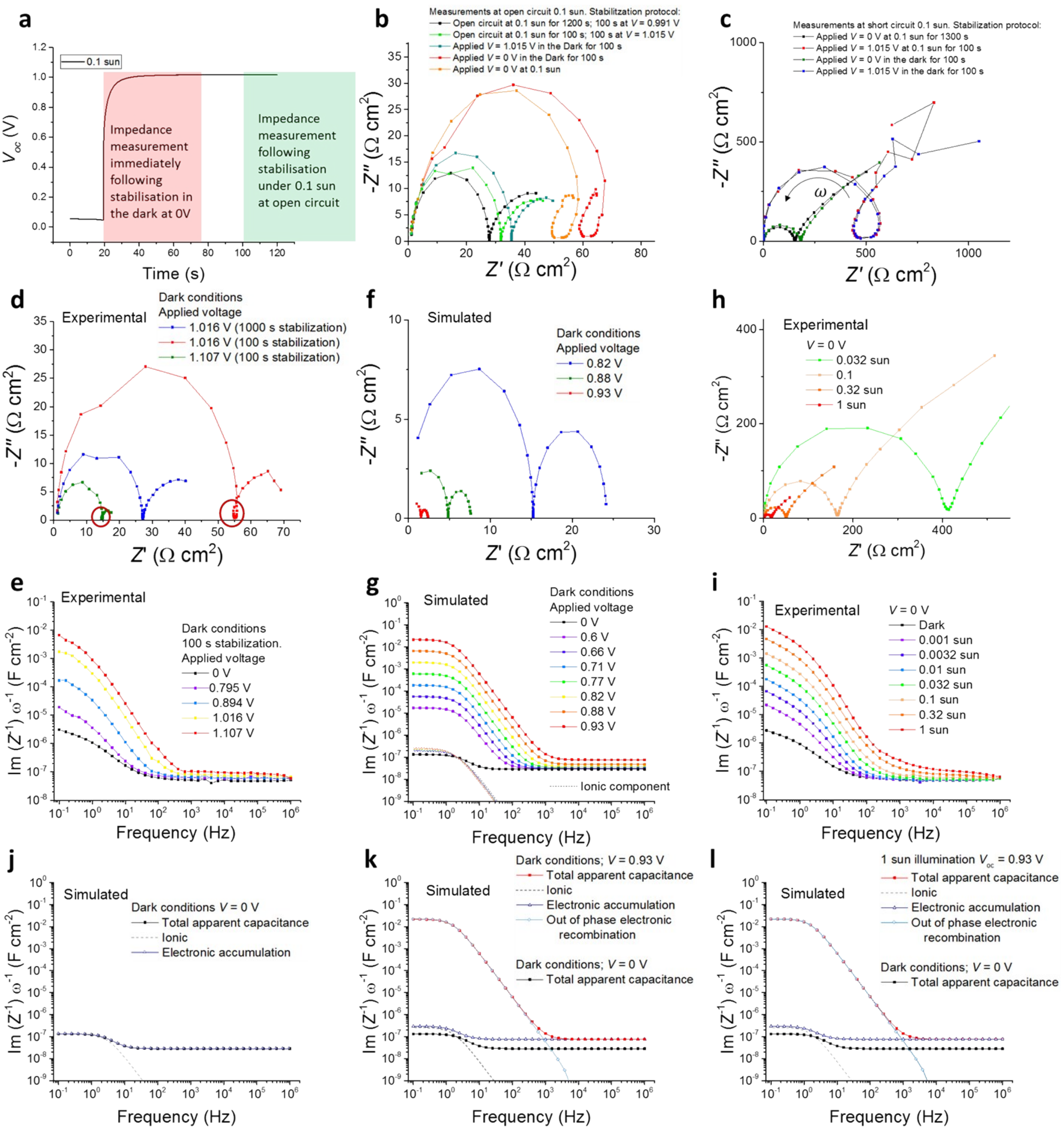

Fig. S2 The effect of stabilisation time, light, and bias voltage in dark on impedance measurements, and the contributions to the apparent capacitance. Measurements performed on the spiro-OMeTAD/ $Cs_{0.05}FA_{0.81}MA_{0.14}PbI_{2.55}Br_{0.45}/TiO_2$ solar cell and the simulated device in Fig. 2. **a**, Measured V_{OC} *vs* time for 0.1 sun illumination following preconditioning at 0 V in the dark. **b**, Measured Nyquist plot of the imaginary *vs* real parts of the impedance over a frequency range 0.1 Hz to 1 MHz, showing effects of different stabilisation protocols prior to measurement at open circuit. **c**, Measured Nyquist plots showing effects of stabilisation protocol for measurements at short circuit. The individual impedance measurements were collected in order of decreasing frequency (opposite direction to arrow). **d - i**, Measured and simulated Nyquist plots and apparent capacitances, $\omega^{-1} Im(Z^{-1})$, against frequency. (**d**, **e**) The effects of bias voltage in the dark for the measured device, and (**f**, **g**) the simulated device. Loops are seen in the measured Nyquist plot (highlighted by the red circles) if the cell was only left to stabilise for 100 s prior to measurement at each voltage, but this loop disappeared if a longer stabilisation period of 1000 s was used prior to measurement. (**h**, **i**) The impedance spectra of the device measured at short circuit with the light intensities indicated in Fig. 2 show qualitatively similar behaviour as at open circuit, though with higher impedances. **j - l**, The different contributions to the apparent capacitance for the device simulated in Fig. 2 and Fig. 3. (**j**) Simulated under dark conditions with zero bias voltage, (**k**) dark with an applied voltage, and (**l**) with 1 sun equivalent conditions at open circuit conditions. Comparison between the electronic accumulation capacitance with an applied voltage or under light at open circuit and the total capacitance evaluated at 0 V in the dark illustrates the effect of the electronic charge in the perovskite on the 'geometric' capacitance (visible experimentally at high frequency in Fig. 2b).

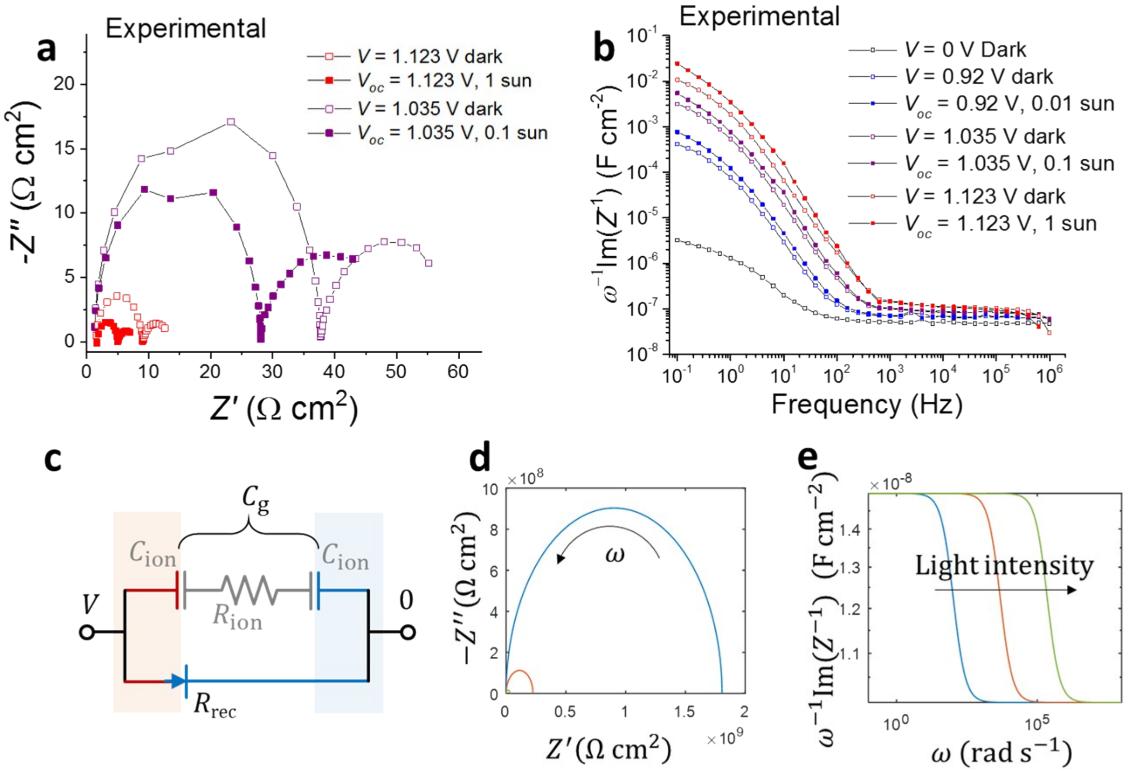

Fig. S3 Possible consequences of photoinduced changes in ionic resistance for impedance spectra of a simplified hybrid perovskite solar cell calculated using an equivalent circuit model assuming C_{ion} is constant. a, **b**, Measured impedance in the light and the dark at the same bias voltage for the device shown in Fig. 2. The results indicate there is modest difference between the (**a**) magnitude of the impedance of the two states which might partly be explained by the consequences of optical heating or drift in cell behaviour (see Fig. S1), although could also be related to an photoinduced change in ionic conductivity[23, 24]. There is also a small change in the apparent capacitance (**b**). **c**, In this equivalent circuit model, the interfacial transistor element seen in Fig. 2e has been replaced with a diode element representing a conventional recombination process. Three light intensities are shown corresponding to potentials V across the device of 0.1 V (blue), 0.2 V (red), and 0.3 V (green) and respective ionic resistances of $R_{\mathrm{ion}} = 2 \times 10^6$, 4×10^4, 1×10^3 Ω cm^2. The other elements are $C_{\mathrm{ion}} = 1 \times 10^{-8}$ F cm^{-2}, $C_{\mathrm{g}} = 1 \times 10^{-8}$ F cm^{-2} and $J_{s1} = 1 \times 10^{-11}$ A cm^{-2}. (**d**) and (**e**) show the resulting modelled impedance and capacitance. It is apparent that although the capacitance of the device shows a shift in its frequency dependence, there is no change in the magnitude of the device capacitance at low frequencies This is in contrast to observation where the apparent capacitance increases at low frequency but there is no significant shift in the frequency of this feature (Fig. 2b and Fig. S1). We note that if there were also photoinduced changes in C_{ion} then it is possible that C_{ion} and R_{ion} could co-vary such that the time constant of the ionic response remained unchanged. However, since C_{ion} will be predominantly controlled by the width of the interfacial space charge regions, which have contributions from both the accumulation/depletion of mobile ions in the perovskite as well as a contribution from depletion of electrons or holes in the contacts. Any change in C_{ion} is likely to be dominated by changes in the electronic depletion layer which to a first approximation scales with $(V_{\mathrm{bi}}/(V_{\mathrm{bi}} - V))^{1/2}$. Thus perfect co-variance of C_{ion} and R_{ion} is unlikely.

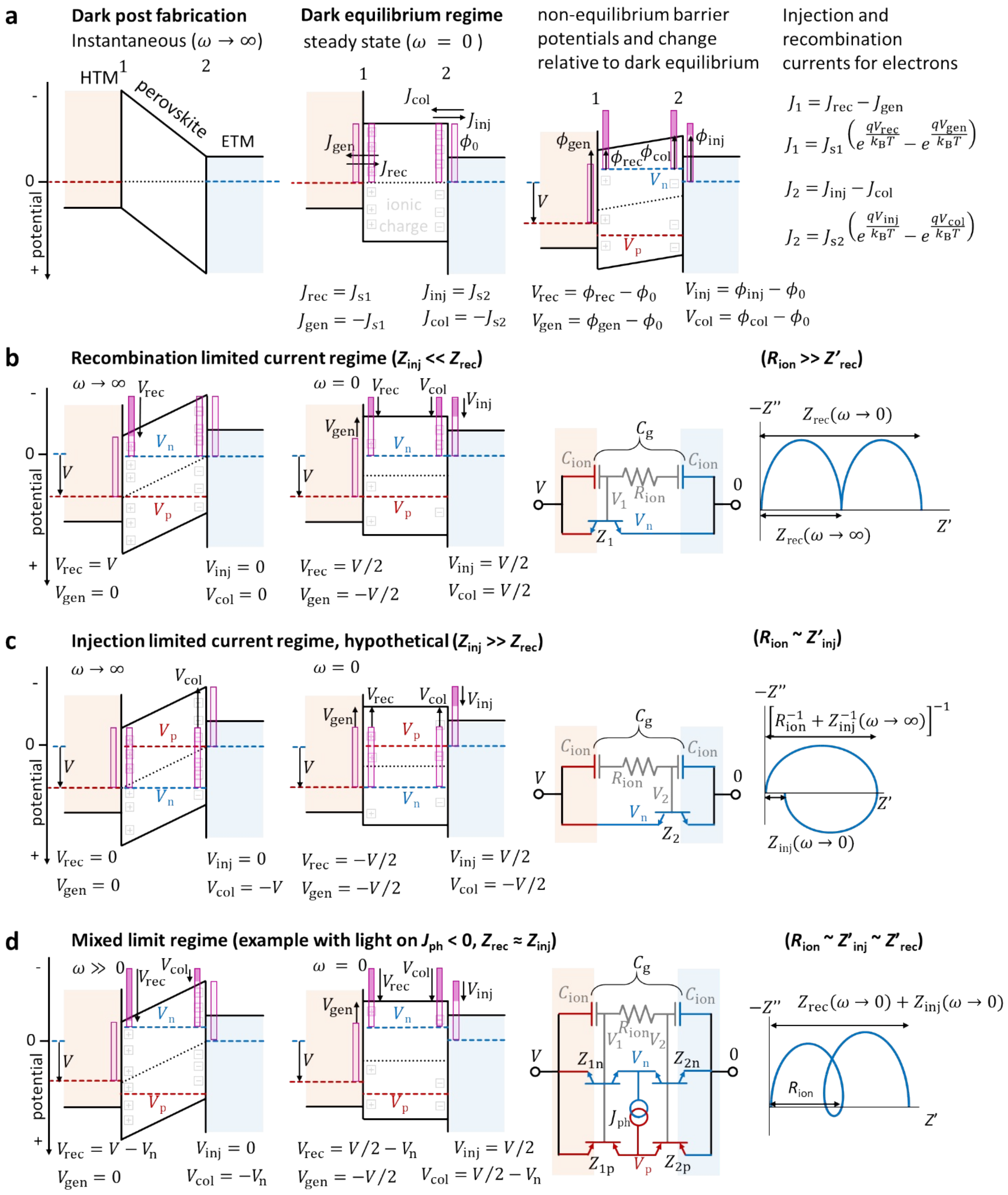

Fig. S4 Simplified energy level diagrams and equivalent circuit models. The conduction and valence bands of the perovskite layer are sandwiched by the hole transporting material (HTM, pink) and the electron transporting material (ETM, light blue), the vertical axis represents electrochemical potential energy which points down. The ionic accumulation layers are assumed negligibly thin. The equilibrium height of the energy barrier for electron injection/collection and recombination/generation in the dark is given by ϕ_0 and ionic charge is represented by the light grey squares. The electron and hole quasi Fermi levels are indicated by the dashed blue and red lines, the other symbols are defined in the main text. The equivalent circuit diagrams are colour coded blue, red and grey to indicate the paths for electrons, holes and ions. **a**, The energy levels of the conduction and valence bands in the dark before and after ionic equilibration. The ideal Schottky-Mott limit electronic energy barriers are indicated, these change with applied potential and ionic redistribution. Energy levels after application of a voltage (V) shown instantaneously ($\omega \to \infty$) and at steady state ($\omega \to 0$) and corresponding circuit models for devices in the: (**b**) recombination limited regime where $J_{s1} << J_{s2}$, (**c**) the injection limited regime where $J_{s1} >> J_{s2}$, and (**d**) the mixed limit regime. Example model Nyquist plots are also shown for each regime, the mixed limit plot corresponds to a special case where R_{ion} is comparable to the real parts of Z_{rec} and Z_{inj}.

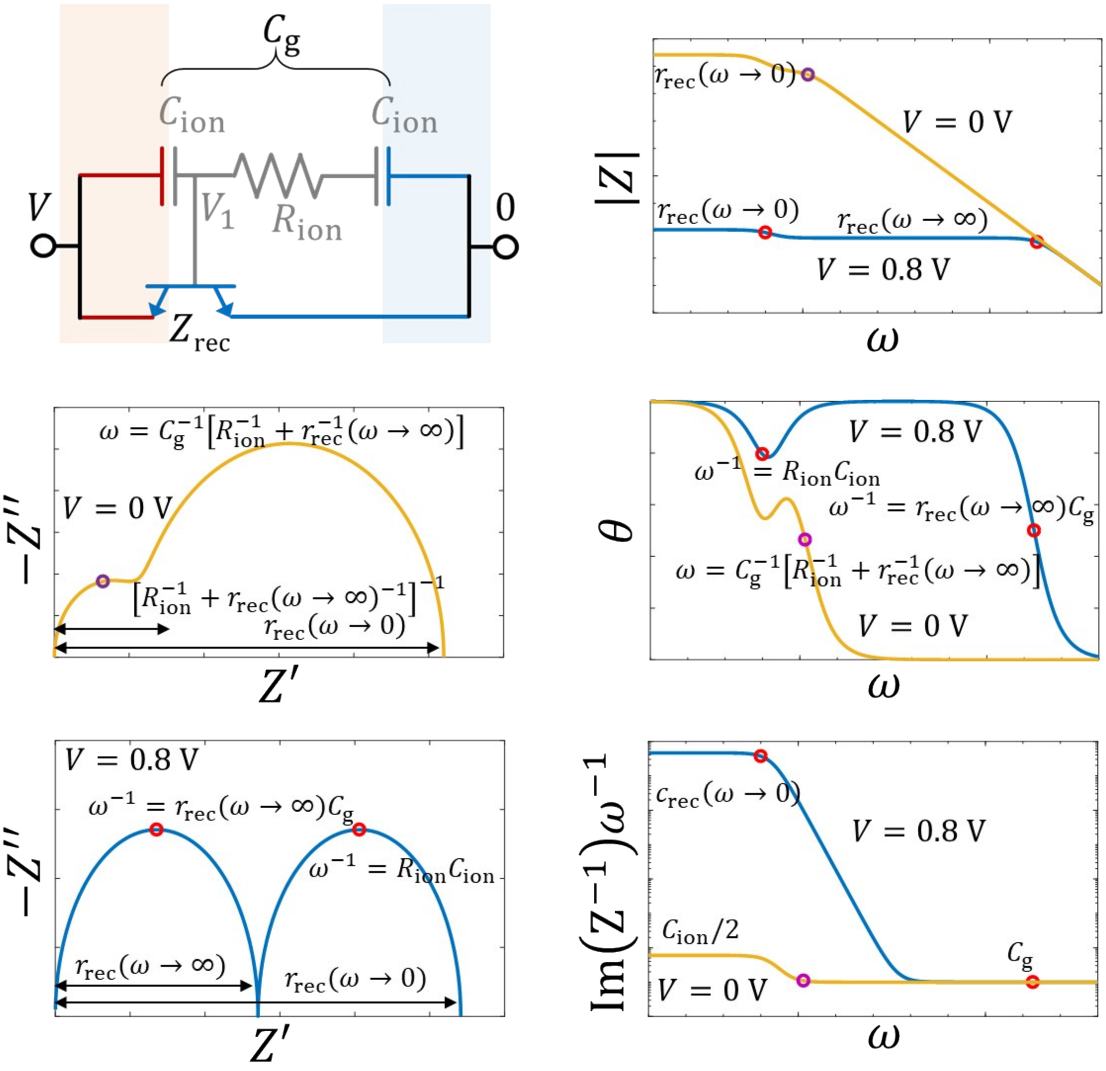

Fig. S5 Interpretation of recombination limited impedance spectra. Example of equivalent circuit model Nyquist plots and impedance spectra (magnitude $|Z(\omega)|$, phase θ, and apparent capacitance $\mathrm{Im}(Z^{-1})\omega^{-1}$ for a recombination limited circuit showing the characteristic time constants at 0 V and 0.8 V. The time constants (ω^{-1}) of various spectral features are indicated corresponding to the coloured circles.

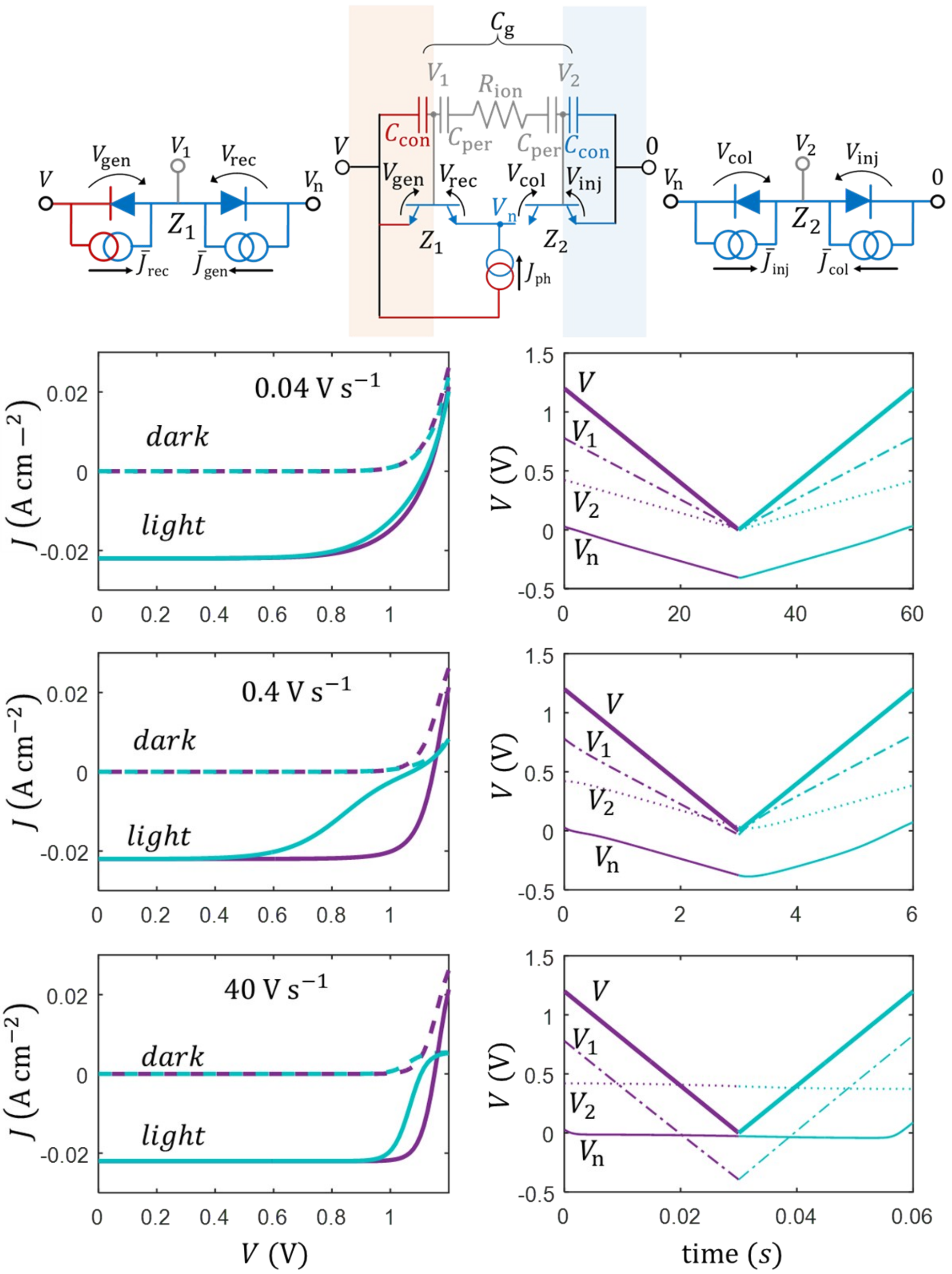

Fig. S6 Circuit model cyclic voltammograms based on parameters from fit to experimental impedance data in Fig. 2. The circuit model is shown above the plots, corresponding to the central column in Fig. S1 (Ebbers-Moll representations[3] of interfacial transistors also shown) with impedance spectroscopy fitting parameters in Table S1 where $C_{ion} = \left[C_{con}^{-1} - C_{per}^{-1}\right]^{-1}$ and $f_c = C_{ion}/C_{con}$. Shown are photogeneration currents J_{ph} = 22 mA cm^{-2} (solid lines) and J_{ph} = 0 (dashed lines) with a scan rates of s = 0.04, 0.4, and 40 V s^{-1} from 1.2 to 0 V for the reverse scan (purple) followed by a forward scan from 0 to 1.2 V (light blue). Applied voltage V, ionic interface potentials V_1 and V_2 and electron potential V_n *vs* time are also shown for the illuminated J_{ph} = 22 mA cm^{-2} cases. The s = 0.4 V s^{-1} case is close to the measured current voltage curve seen in Fig. S8.

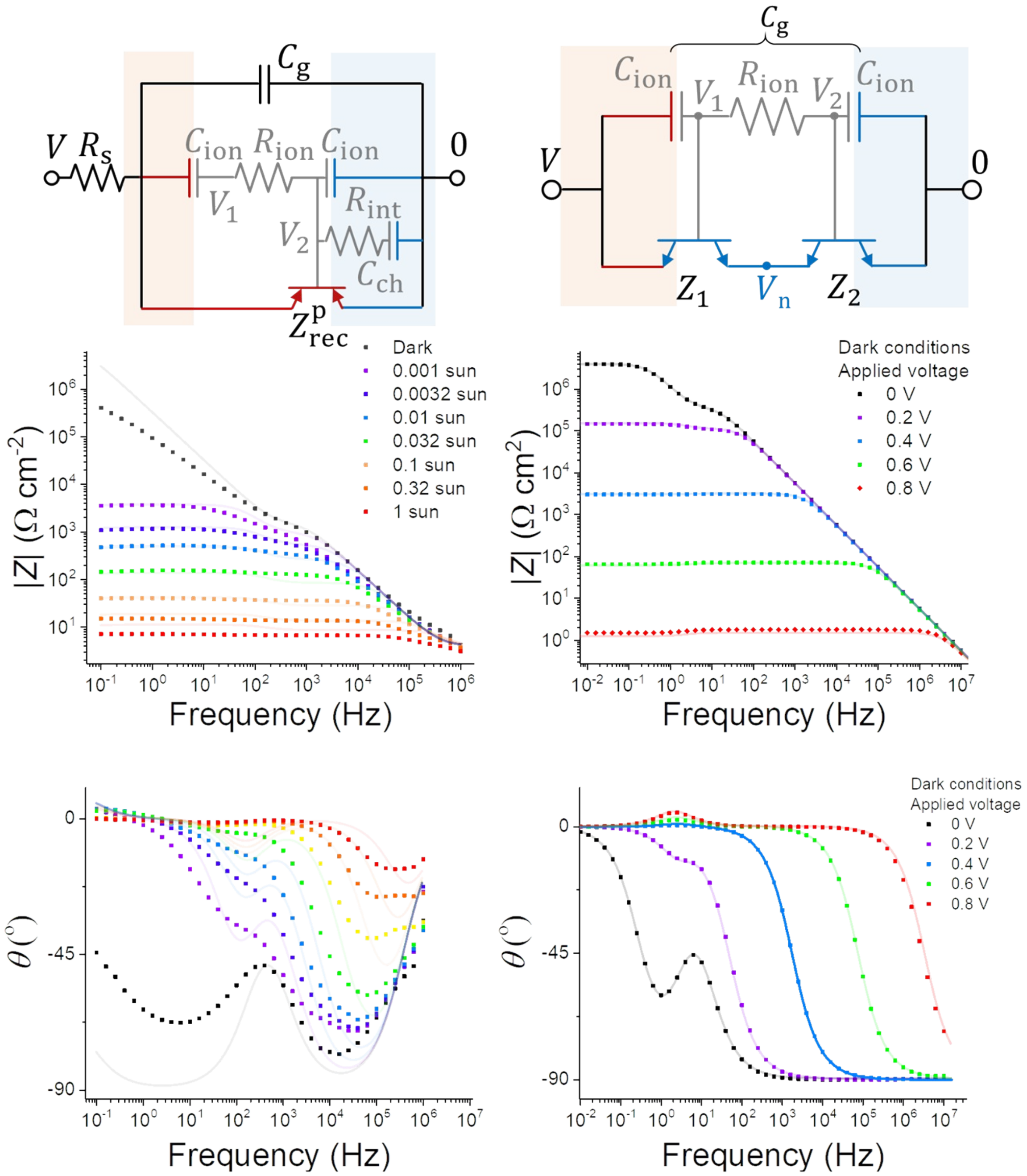

Fig. S7 Circuit models and complete impedance spectra corresponding to Fig. 5a (left-hand column) and Fig. 5b (right-hand column). The solid lines show the global fit to all the data using the parameters listed in Table S1. The left-hand column shows a global fit to the impedance measurements of the spiro-OMeTAD/ $FA_{0.85}MA_{0.15}PbI_3/SnO_x$ in Fig. 5a (measured around open circuit with different bias light intensities, see Methods and Table S1 caption for V_{OC} values) assuming a model in which ions may penetrate or reversibly react at the recombination interface. The drift diffusion model parameters used to create the simulated impedance measurements in the right-hand column (Fig. 5b) are identical to those listed in Table S2 except that the recombination lifetimes of the contacts were reduced by 10,000 times so that $\tau_n = \tau_p = 5 \times 10^{-14}$ s, and the mobility of the majority carrier species in the contacts were reduced by 100 times so that $\mu_h = 0.2$ cm^2 V^{-1} s^{-1} in the p-type contact and $\mu_e = 0.2$ cm^2 V^{-1} s^{-1} in the n-type contact.

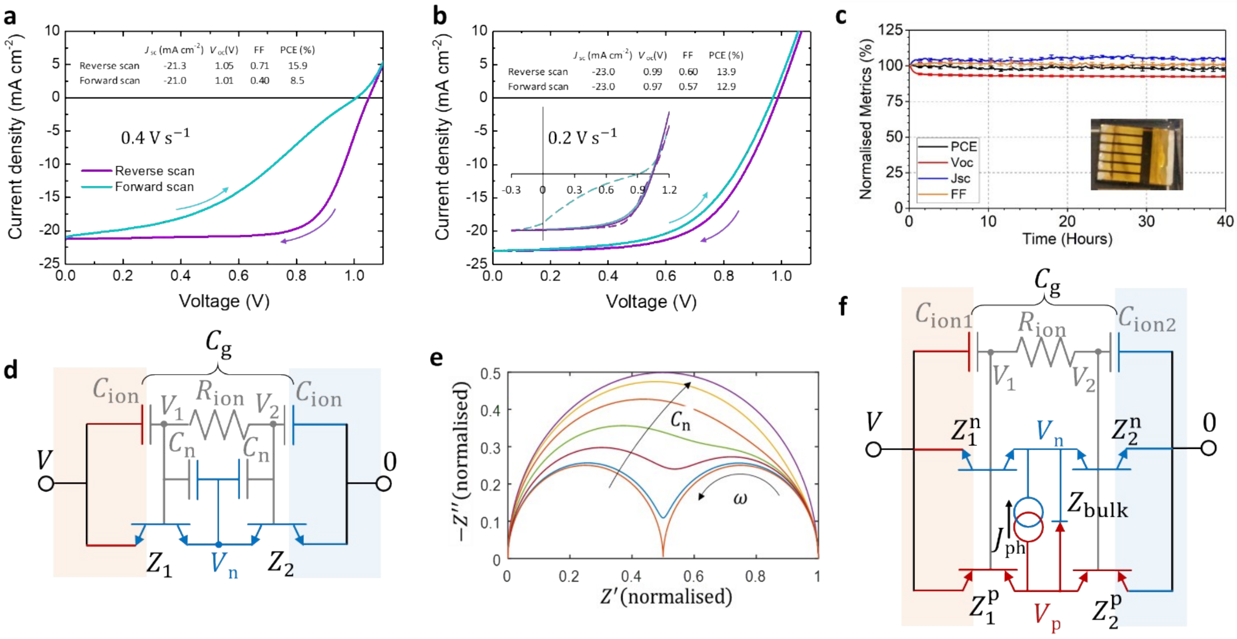

Fig. S8 Solar cell data and circuit models described in the Methods and Note S3. a, Current-voltage sweeps of the spiro-OMeTAD/ $Cs_{0.05}FA_{0.81}MA_{0.14}PbI_{2.55}Br_{0.45}/TiO_2$ solar cell in Fig. 2a and b measured under AM1.5 illumination with a sweep rate of 0.4 V s^{-1}. **b**, Current-voltage sweeps of the spiro-OMeTAD/ $FA_{0.85}MA_{0.15}PbI_3/SnO_2$ solar cell in Fig. 5a measured under AM1.5 illumination with a sweep rate of 0.2 V s^{-1}. For comparison the inset shows cyclic voltamograms for both cells (**a** -dashed lines, **b** - solid lines) measured both measured with a continuous 0.2 V s^{-1} sweep cycle under the white LEDs (one sun equivalent, normalised photocurrent) used for the impedance measurements. **c**, Normalised power conversion efficiency (PCE), V_{OC}, short circuit current (J_{SC}), and fill factor (FF) as a function of illumination time of a device prepared using the same procedure as that measured in **a**. **d**, Equivalent circuit model including the effects of screening by electrons in the perovskite on the interfacial capacitances (C_n). **e**, Normalised Nyquist plot, calculated from the circuit model shown in **d**, indicating the effect of increasing C_n on the shape of the spectrum. The example is calculated with the same parameters as those shown in Fig. S5 where $J_{s1} << J_{s2}$ with an applied voltage of 0.5 V, and varying C_n from 10^{-12} – 10^{-7} F cm^{-2}. **f**, A general solar cell circuit model including, free electrons and holes, photogeneration, and the effects of bulk recombination.

Supplementary Tables

Table S1. Global fit parameters for the measured and simulated impedance data presented in the study. The applied voltages used as inputs for the circuit model (Fig. 2e) of the experimental data in Fig. 2a and b (also Fig. S1b and c) were: 1.107 V (1 sun), 1.066 V (0.32 sun), 1.016 V (0.1 sun), 0.955 V (0.032 sun), 0.894 V (0.01 sun), 0.846 V (0.0032 sun), 0.795 V (0.001 sun) with a steady state ideality factor of m_{ss} = 1.79. The applied voltages for the simulated measurements in Fig. 2c and d were: 0.931 V (1 sun), 0.876 V (0.32 sun), 0.822 V (0.1 sun), 0.766 V (0.032 sun), 0.711 V (0.01 sun), 0.656 V (0.0032 sun), 0.600 V (0.001 sun) with a steady state ideality factor of m_{ss} = 1.84, V_{bi} = 1.3 V. * The value inferred from the simulation input parameters is $R_{ion} = d_{intrinsic}/(q\mu_a N_{ion})$ = 3.1 ×10^5 Ω cm^2, close to the value extracted from the fit to the simulated impedance measurements using the expression $R_{ion} = c_{rec}(\bar{V})4m_{ss}(1-f_c/2)k_BT/(qf_cC_{ion}J_{rec}(\bar{V}))$ = 3.8 ×10^5 Ω cm^2 (see main text, and, for the experimental data the inset in Fig. 2b). The deviation between the simulation input value and the fit value of R_{ion} in the table below arises due to factors not accounted for by the circuit model which the fit attempts to compensate for, particularly the capacitive screening of interfaces by the electronic charge at the higher light intensities (see Note S3). The applied voltages used as inputs to the circuit model (Fig. S7, left column) for the experimental data in Fig. 5a were: 1.061 V (1 sun), 1.012 V (0.32 sun), 0.948 V (0.1 sun), 0.865 V (0.032 sun), 0.777 V (0.01 sun), 0.713 V (0.0032 sun), 0.638 V (0.001 sun), with a steady state ideality factor of m_{ss} = 2.43. The applied voltages used as inputs for the circuit model (Fig. 4g, Fig. S7, right column) of the simulated impedance measurements in Fig. 5b were: 0, 0.2, 0.4, 0.6, and 0.8 V, with a steady state ideality factor of m_{ss} = 1.93. The ideality factor for charge injection/collection was assumed to be unity. Fit uncertainties approximately correspond to the number of decimal places shown.

Parameter	**Experimental data (Fig. 2a,b)**	**Simulated data (Fig. 2c,d)**	**Experimental data (Fig. S1d-f)**	**Experimental data (Fig. 5a)**	**Simulated data (Fig. 5b)**
R_s (Ω cm^2)	-	-	-	3.2	-
C_g (F cm^{-2})	4.4×10^{-8}	2.8×10^{-8}	4.4×10^{-8}	1.0×10^{-7}	2.8×10^{-8}
R_{ion} (Ω cm^2)	6.7×10^{4}	3.8×10^{5} *	6.7×10^{4}	2.2×10^{3}	3.8×10^{5}
R_{int} (Ω cm^2)	-	-	-	4.1×10^{6}	-
C_{ion} (F cm^{-2})	7.2×10^{-6}	2.6×10^{-7}	7.2×10^{-6}	8.6×10^{-7}	2.6×10^{-7}
C_{con} (F cm^{-2})	-	-	-	7.8×10^{-7}	-
J_{s1} (A cm^{-2})	6.1×10^{-13}	7.1×10^{-11}	7.0×10^{-13}	-	1.19×10^{-8}
J_{s2} (A cm^{-2})	-	-	3.1×10^{-9}	6.0×10^{-9}	1.50×10^{-8}
f_c	0.70	0.77	0.70	0.65	0.996

Table S2 **Drift-diffusion simulation parameters.** These parameters were used for all the simulated data (simulated as described in reference [25]), except where explicitly stated. The 1 sun equivalent V_{OC} resulting from this parameters set is 0.931 V, the resulting J_{SC} is 20.3 mA/cm^2.

Parameter name	**Symbol**	**p-type**	**Intrinsic**	**n-type**	**Unit**
Layer thickness	d	200	500	200	nm
Band gap	E_g	1.6	1.6	1.6	eV
Built in voltage	V_{bi}	1.3	1.3	1.3	V
Relative dielectric constant	ε_s	20	20	20	
Mobile ionic defect density	N_{ion}	0	10^{19}	0	cm^{-3}
Ion mobility	μ_a	-	10^{-10}	-	cm^2 V^{-1} s^{-1}
Electron mobility	μ_e	0.02	20	20	cm^2 V^{-1} s^{-1}
Hole mobility	μ_h	20	20	0.02	cm^2 V^{-1} s^{-1}
Donor doping density	N_A	3.0×10^{17}	-	-	cm^{-3}
Acceptor doping density	N_D	-	-	3.0×10^{17}	cm^{-3}
Effective density of states	N_0	10^{20}	10^{20}	10^{20}	cm^{-3}
Band-to-band recombination rate coefficient	k_{btb}	10^{-12}	10^{-12}	10^{-12}	cm^{-3} s^{-1}
SRH trap energy	E_t	E_{CB}-0.8	-	E_{CB}-0.8	eV
SRH time constants	τ_n, τ_p	5×10^{-10}	-	5×10^{-10}	s
Generation rate	G	-	2.5×10^{21}	-	cm^{-3} s^{-1}

Table S3. Changes in interfacial barrier potentials and small perturbation impedances due to ionic redistribution considering only free electrons. The terms in the equations are described in the main text, Note S2 and illustrated in Fig. 4g and Fig. S4. In the small perturbation regime an oscillating voltage v is superimposed on the steady state cell bias potential $\bar{V}$. Complete expressions considering holes are given in the in Table S4 and Note S6, considering asymmetric interfacial capacitances, and screening within the perovskite. The symbols covered by a bar (e.g. $\bar{V}$) indicate the steady state value of the at quantity when $\omega \to 0$. *Assumes that mobile ionic charge does not penetrate or react at interfaces and the C_{ion} is the same at each interface.

Change in barrier potential for:	**(V)**		**(V)**		**response to small voltage perturbation, *v* (V)**
Electron generation	V_{gen}	=	$V_1 - V$	=	$-\bar{V}\bar{A} - vA$
Electron recombination	V_{rec}	=	$V_1 - V_n$	=	$\bar{V}\left(1 - \bar{A} - \bar{B}_n\right) + v\left(1 - A - B_n\right)$
Electron collection	V_{col}	=	$V_2 - V_n$	=	$\bar{V}\left(\bar{A} - \bar{B}_n\right) + v(A - B_n)$
Electron injection	V_{inj}	=	V_2	=	$\bar{V}\bar{A} + vA$
Small voltage perturbation parameters					
Fraction of ionic screening potential within contact layer	f_c	=	$1 - \frac{C_{ion}}{C_{per}}$	=	$1 - \frac{total\ interface\ capacitance}{perov.\ space\ charge\ capacitance}$
Fraction of voltage change at interface due to ionic redistribution*	A	=	$\frac{v_C}{v}$	=	$\frac{f_c}{2 + i\omega R_{ion} C_{ion}}$
Potential due to ions at interface 1 (V)			v_1	=	$v(1 - A)$
Potential due to ions at interface 2 (V)			v_2	=	vA
Fractional change in voltage of electron quasi Fermi level	B_n	=	$\frac{v_n}{v}$	=	$\frac{\bar{J}_{rec} + A\left(\bar{J}_{gen} - \bar{J}_{rec} + \bar{J}_{col} - \bar{J}_{inj}\right)}{\bar{J}_{rec} + \bar{J}_{col}}$
Interfacial currents					**(A cm⁻²)**
Electron generation			J_{gen}	=	$J_{s1} e^{\frac{qV_{gen}}{m_1 k_B T}}$
Electron recombination			J_{rec}	=	$J_{s1} e^{\frac{qV_{rec}}{m_1 k_B T}}$
Electron collection			J_{col}	=	$J_{s2} e^{\frac{qV_{col}}{m_2 k_B T}}$
Electron injection			J_{inj}	=	$J_{s2} e^{\frac{qV_{inj}}{m_2 k_B T}}$
Interfacial impedances					**(Ω cm^2)**
Electron generation impedance			Z_{gen}	=	$\frac{\left(1 - B_n\right) m_1 k_B T}{A \quad q\bar{J}_{gen}}$

Electron recombination impedance	Z_{rec}	$=$	$\frac{(1-B_n)\ \ m_1k_BT}{(1-A-B_n)\ \ q\bar{J}_{rec}}$
Interface 1 electron impedance	Z_1	$=$	$\left(\frac{1}{Z_{rec}}+\frac{1}{Z_{gen}}\right)^{-1}$
Electron collection impedance	Z_{col}	$=$	$\frac{B_n\ \ m_2k_BT}{(B_n-A)\ \ q\bar{J}_{col}}$
Electron injection impedance	Z_{inj}	$=$	$\frac{B_nm_2k_BT}{A\ \ q\bar{J}_{inj}}$
Interface 2 electron impedance	Z_2	$=$	$\left(\frac{1}{Z_{inj}}+\frac{1}{Z_{col}}\right)^{-1}$

Table S4. Changes in interfacial barrier potentials and small perturbation impedances due to ionic redistribution considering both free electrons and holes, and including bulk recombination. The superscripts n and p are used to processes involving free electrons or holes respectively, *they are not exponents*. The terms in the equations are described in the main text and illustrated in Fig. 4. In the small perturbation regime an oscillating voltage v is superimposed on the cell potential V. The electron and hole quasi Fermi levels, V_n and V_p have corresponding small perturbation oscillations v_n and v_p. The ideality factors of interface 1 and 2 are given by m_1 and m_2 respectively. A_1 and A_2 arise because the capacitances of each interface are different, C_ion1 and C_ion2. The symbols covered by a bar (e.g. $\bar{V}$) indicate the steady state value of the quantity when $\omega \rightarrow 0$. *Assumes that mobile ionic charge does not penetrate or chemically react at interfaces.

Change in barrier potential for:			**(V)**		**Response to small voltage perturbation, *v* (V)**
Electron generation	V_{gen}^{n}	=	$V_1 - V$	=	$-\bar{V}\bar{A}_1 - vA_1$
Electron recombination	V_{rec}^{n}	=	$V_1 - V_n$	=	$\bar{V}\left(1 - \bar{A}_1 - \bar{B}_n\right) + v\left(1 - A_1 - B_n\right)$
Electron collection	V_{col}^{n}	=	$V_2 - V_n$	=	$\bar{V}(\bar{A}_2 - \bar{B}_n) + v(A_2 - B_n)$
Electron injection	V_{inj}^{n}	=	V_2	=	$\bar{V}\bar{A}_2 + vA_2$
Hole generation	V_{gen}^{p}	=	$-V_2$	=	$-\bar{V}\bar{A}_2 - vA_2$
Hole recombination	V_{rec}^{p}	=	$V_p - V_2$	=	$\bar{V}\left(\bar{B}_p - \bar{A}_2\right) + v\left(B_p - A_2\right)$
Hole collection	V_{col}^{p}	=	$V_p - V_1$	=	$\bar{V}\left(\bar{B}_p + \bar{A}_1 - 1\right) + v\left(B_p + A_1 - 1\right)$
Hole injection	V_{inj}^{p}	=	$V - V_1$	=	$\bar{V}\bar{A}_1 + vA_1$
Bulk recombination	V_{bulk}	=	$V_p - V_n$	=	$\bar{V}\left(\bar{B}_p - \bar{B}_n\right) + v\left(B_p - B_n\right)$

Small voltage perturbation parameters					
Fraction of ionic screening potential within contact layers	f_c	=	$1 - \frac{C_{ion}}{C_{per}}$	=	$1 - \frac{total\ interface\ capacitance}{perov.\ space\ charge\ capacitar}$
Fraction voltage change at interface 1 due ion redistribution*	A_1	=	$\frac{v_{C_{ion1}}}{v}$	=	$\frac{f_c}{1 + C_{ion1}/C_{ion2} + i\omega R_{ion}C_{ion1}}$
Fraction voltage change at interface 2 due ion redistribution*	A_2	=	$\frac{v_{C_{ion2}}}{v}$	=	$\frac{f_c}{1 + C_{ion2}/C_{ion1} + i\omega R_{ion}C_{ion2}}$
Potential due to ions at interface 1 (V)			v_1	=	$v(1 - A_1)$
Potential due to ions at interface 2 (V)			v_2	=	vA_2
Fractional change in voltage of electron quasi Fermi level	B_n	=	$\frac{v_n}{v}$	=	Lengthy analytical expression, solved using Kirchhoff's laws
Fractional change in voltage of hole quasi Fermi level	B_p	=	$\frac{v_p}{v}$	=	Lengthy analytical expression, solved using Kirchhoff's laws

Interfacial currents		**(A cm^{-2})**
Ideality factor of interface 1	m_1	

Ideality factor of interface 2	m_2		
Electron generation	J_{gen}^{n}	=	$J_{s1}e^{\frac{qV_{gen}^{n}}{m_1k_BT}}$
Electron recombination	J_{rec}^{n}	=	$J_{s1}e^{\frac{qV_{rec}^{n}}{m_1k_BT}}$
Electron collection	J_{col}^{n}	=	$J_{s2}e^{\frac{qV_{col}^{n}}{m_2k_BT}}$
Electron injection	J_{inj}^{n}	=	$J_{s2}e^{\frac{qV_{inj}^{n}}{m_2k_BT}}$
Hole generation	J_{gen}^{p}	=	$J_{s1}e^{\frac{qV_{gen}^{p}}{m_2k_BT}}$
Hole recombination	J_{rec}^{p}	=	$J_{s1}e^{\frac{qV_{rec}^{p}}{m_2k_BT}}$
Hole collection	J_{col}^{p}	=	$J_{s2}e^{\frac{qV_{col}^{p}}{m_1k_BT}}$
Hole injection	J_{inj}^{p}	=	$J_{s2}e^{\frac{qV_{inj}^{p}}{m_1k_BT}}$
Bulk recombination	J_{bulk}	=	$J=J_0\left(e^{\frac{qV_{bulk}}{k_BT}}-1\right)$

Interfacial impedances			**(Ω cm²)**
Electron generation impedance	Z_{gen}^{n}	=	$\frac{(1-B_n)m_1k_BT}{A_1\ \ q\bar{J}_{gen}^{n}}$
Electron recombination impedance	Z_{rec}^{n}	=	$\frac{(1-B_n)\ \ m_1k_BT}{(1-A_1-B_n)\ q\bar{J}_{rec}^{n}}$
Interface 1 electron impedance	Z_{1}^{n}	=	$\left(\frac{1}{Z_{rec}^{n}}+\frac{1}{Z_{gen}^{n}}\right)^{-1}$
Electron collection impedance	Z_{col}^{n}	=	$\frac{B_n\ \ m_2k_BT}{(B_n-A_2)\ q\bar{J}_{col}^{n}}$
Electron injection impedance	Z_{inj}^{n}	=	$\frac{B_nm_2k_BT}{A_2\ q\bar{J}_{inj}^{n}}$
Interface 2 electron impedance	Z_{2}^{n}	=	$\left(\frac{1}{Z_{inj}^{n}}+\frac{1}{Z_{col}^{n}}\right)^{-1}$
Hole generation impedance	Z_{gen}^{p}	=	$\frac{B_pm_2k_BT}{A_2\ q\bar{J}_{gen}^{p}}$

Hole recombination impedance	Z_{rec}^{p}	=	$\frac{B_p \quad m_2 k_B T}{(B_p - A_2) \;\; q\bar{J}_{rec}^{p}}$
Interface 2 hole impedance	Z_2^p	=	$\left(\frac{1}{Z_{rec}^{p}} + \frac{1}{Z_{gen}^{p}}\right)^{-1}$
Hole collection impedance	Z_{col}^{p}	=	$\frac{(1 - B_p) \quad m_1 k_B T}{(1 - A_1 - B_p) \;\; q\bar{J}_{col}^{p}}$
Hole injection impedance	Z_{inj}^{p}	=	$\frac{(1 - B_p) m_1 k_B T}{A_1 \quad q\bar{J}_{inj}^{p}}$
Interface 1 hole impedance	Z_1^p	=	$\left(\frac{1}{Z_{inj}^{p}} + \frac{1}{Z_{col}^{p}}\right)^{-1}$
Bulk recombination impedance	Z_{bulk}	=	$\frac{k_B T}{q\bar{J}_{bulk}}$
Impedance of hole circuit branch	Z_p	=	$Z_1^p + Z_2^p$
Impedance of electron circuit branch	Z_n	=	$Z_1^n + Z_2^n$
Total impedance of active layer interfaces	Z_{np}	=	$\left(\frac{1}{Z_n} + \frac{1}{Z_p}\right)^{-1}$